Photochemical & Photobiological Sciences (2024) 23:31–53
https://doi.org/10.1007/s43630-023-00496-0

ORIGINAL PAPERS

Merocyanines form bacteriorhodopsins with strongly bathochromic absorption maxima

Megan J. Mackintosh[1] · Dorothee Hoischen[2,4] · Hans-Dieter Martin[2] · Igor Schapiro[1] · Wolfgang Gärtner[3]

Received: 26 July 2023 / Accepted: 13 October 2023 / Published online: 9 December 2023

Abstract

There is a need to shift the absorbance of biomolecules to the optical transparency window of tissue for applications in optogenetics and photo-pharmacology. There are a few strategies to achieve the so-called red shift of the absorption maxima. Herein, a series of 11 merocyanine dyes were synthesized and employed as chromophores in place of retinal in bacteriorhodopsin (bR) to achieve a bathochromic shift of the absorption maxima relative to bR's λ^a_{max} of 568 nm. Assembly with the apoprotein bacterioopsin (bO) led to stable, covalently bound chromoproteins with strongly bathochromic absorbance bands, except for three compounds. Maximal red shifts were observed for molecules **9**, **2**, and **8** in bR where the λ^a_{max} was 766, 755, and 736 nm, respectively. While these three merocyanines have different end groups, they share a similar structural feature, namely, a methyl group which is located at the retinal equivalent position 13 of the polyene chain. The absorption and fluorescence data are also presented for the retinal derivatives in their aldehyde, Schiff base (SB), and protonated SB (PSB) forms in solution. According to their hemicyanine character, the PSBs and their analogue bRs exhibited fluorescence quantum yields (Φ_f) several orders of magnitude greater than native bR (Φ_f 0.02 to 0.18 versus 1.5×10^{-5} in bR) while also exhibiting much smaller Stokes shifts than bR (400 to 1000 cm^{-1} versus 4030 cm^{-1} in bR). The experimental results are complemented by quantum chemical calculations where excellent agreement between the experimental λ^a_{max} and the calculated λ^a_{max} was achieved with the second-order algebraic-diagrammatic construction [ADC(2)] method. In addition, quantum mechanics/molecular mechanics (QM/MM) calculations were employed to shed light on the origin of the bathochromic shift of merocyanine **2** in bR compared with native bR.

This publication is dedicated to Dr. Silvia E. Braslavsky as her amazing journey through science brought her to a memorable landmark.

Hans-Dieter Martin passed away on March 8, 2009.

✉ Igor Schapiro
igor.schapiro@mail.huji.ac.il

✉ Wolfgang Gärtner
wolfgang.gaertner@uni-leipzig.de

[1] Fritz Haber Center for Molecular Dynamics, Institute of Chemistry, The Hebrew University of Jerusalem, Jerusalem, Israel

[2] Institute for Organic Chemistry and Macromolecular Chemistry, University of Düsseldorf, 40225 Düsseldorf, Germany

[3] Institute of Analytical Chemistry, 04103 Leipzig, Germany

[4] Present Address: ISK Biosciences Europe N.V., 1831 Diegem, Belgium

Graphical abstract

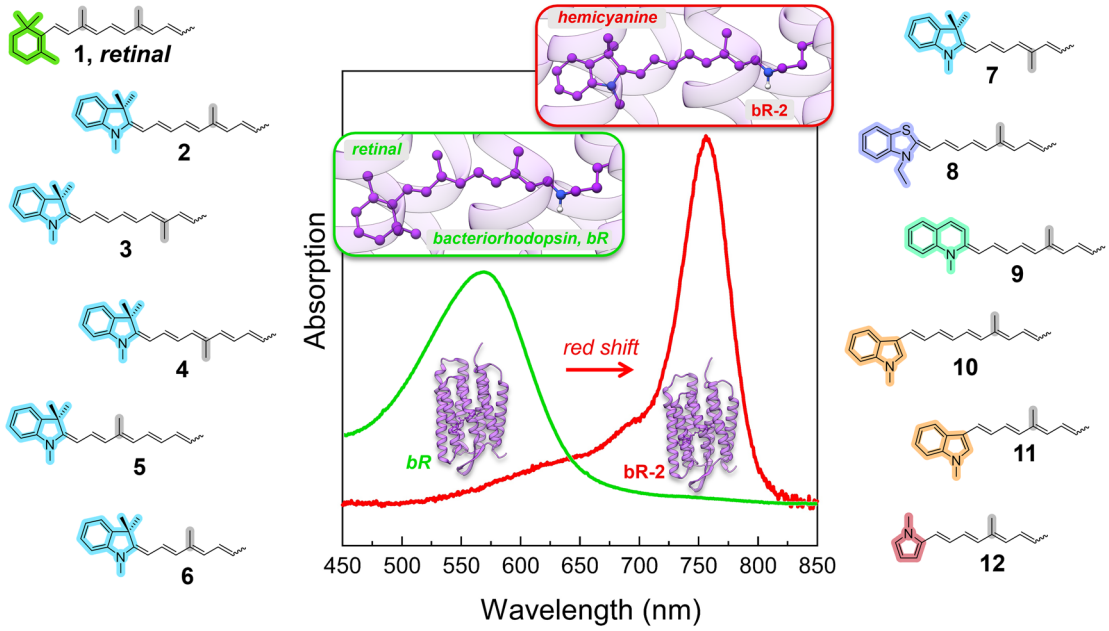

Keywords Bacteriorhodopsin · Retinal · Merocyanines · Photocycle · TD-DFT · ADC(2) · Hybrid QM/MM · Schiff base

Abbreviations

bO	Bacterioopsin
bR	Bacteriorhodopsin
DIBAH	Diisobutylaluminium hydride
mp	Melting point
OS	Opsin shift
(P)SB	(Protonated) Schiff base

1 Introduction

The embedding of ligands into proteins represents the transfer from the homogeneous solvent into the strongly heterogeneous environment composed of amino acids. Such process alters the chemical properties of the ligand to a large extent—even more so—in chromoproteins, where the incorporation of the chromophore may cause a strong alteration of the position (λ^a_{max}) and intensity (ε_{max}) of the absorption band as well as the photochemical properties of the chromophore. In the light-activated, retinal-containing membrane protein bacteriorhodopsin (bR) from the Archaeon *Halobacterium salinarum*, the quantum yield, the selectivity of the photoisomerization of one particular double bond of the retinal chromophore, and also the spectral position of the absorption bands are efficiently tuned by the protein [1–4]. In particular, the latter property, i.e., the formation of a chromophoric system which absorbs light in the visible range, contrasts the absorption of the retinal chromophore in ethanol solution which peaks in the ultraviolet spectral range ($\lambda^a_{max(EtOH)} = 380$ nm). This is an obvious consequence of specific chromophore–protein interactions. The strong red shift of the absorption band ($\lambda^a_{max(bR)} = 568$ nm) upon binding of the retinal chromophore to the apoprotein bacterioopsin (bO), via the formation of a protonated Schiff base (PSB) to Lys216, is referred to as the opsin shift (OS) [5]. The OS was initially proposed by Honig and coworkers and is defined by the difference in the absorption of the protonated retinal-butylamine Schiff base in solution (mostly measured-as here-in EtOH and using HCl as acid) and the PSB in bR [5]

$$\text{OS}\ (\text{cm}^{-1}) = \lambda^a_{max,PSB}\ (\text{cm}^{-1}) - \lambda^a_{max,bR}\ (\text{cm}^{-1}).$$

In general, based on studies of bR and visual opsins, the following factors contribute to the OS:

(i) The first being the distribution of the positive charge of the PSB along the polyene chain of the chromophore [6, 7].
(ii) The influence of the protein environment on the chromophore plays an important role in the degree of the OS [5, 8–14]. For example, Kropf and Hubbard first suggested that charged amino acids near the chromophore could be key to the observed shifts between the λ_{max} of retinal in solution versus the pro-

tein environment [8]. Later, Honig, Nakanishi, and coworkers presented formative studies on the role of charged and polar residues near the PSB of retinal for bR and visual opsins [10, 11]. Their work also considered charged or polar amino acids in vicinity to the cyclohexenyl ring of the chromophore as modulating factor ('external two point charge model'). Dispersion interactions also impact the OS and have been reported in several experimental and computational studies [13–17].

(iii) The twist of the bonds can also impact the OS [13, 14, 18–21]. There are two potential ways to achieve this. The first is a conformational change between 6-s-*cis* and 6-s-*trans* which determines the twist between the cyclohexene ring and the retinal polyene. It induces a change in the conjugation of the ring's double bond with the π-system of the polyene chain which has been shown to shift the absorption maximum by 80 nm in recent measurements of retinal analogues. Second, the twist of the polyene chain's double or single bonds inducing a red shift or a blue shift, respectively.

Many of these interactions between the chromophore and selected amino acids of the protein are well understood, since highly resolved three-dimensional structures of bR [22] and of some of the photocycle intermediates are now available [23].

To validate specific interactions between chromophore and protein as well as to quantify their effect, site-directed mutagenesis has been used. In addition, chemically synthesized, structurally modified chromophores have yielded valuable information not obtainable by mutagenesis [19, 24–28]. As the vertebrate rhodopsins carry the 11-*cis* isomer of the same chromophore, structurally and electronically modified retinal derivatives have been employed in several pigments, light-driven ion pumps, *e.g.,* bR and halorhodopsin (hR), microbial rhodopsins, and also their animal counterparts [24, 29–33]. Besides the introduction of sterically and electronically modified substituents into the retinal structure [19, 34], changes of the cyclohexenyl ring moiety have been accomplished. A cornerstone was the fixation of the ring structure in 6-*s*-*cis* (confirming the structure in animal rhodopsin) and alternatively in 6-*s*-*trans* (thereby demonstrating by the large bathochromically shifted absorption maximum that this structure is valid for bR) [19]. Further structural changes were placement of an aromatic ring system instead of the cyclohexenyl ring [34], an azulene or a merocyanine compound (which upon formation of a PSB converts into a hemicyanine structure) [35, 36]. Early attempts to extend the wavelength range of bO were based on the polarized double bond system of retinal in which position with odd numbers (13, 11, 9) carry a slightly positive charge, whereas even positions (14, 12, 10) are more negative [37]. Accordingly, this polarization became stronger by the introduction of halide substituents at positions 12, 13, or 14 of retinal yielding a noticeable red shift of the absorption band upon assembly with bO, and theoretical calculations revealed that the SB protonation causes a slight elongation of the 13–14 double bond and a constriction of the 14–15 single bond [32, 35, 37, 38]. Much stronger bathochromic absorption maxima resulted, when push–pull systems were introduced such as, in the simplest case, by exchanging of the cyclohexenyl ring of retinal by a piperidine moiety [39]. These scholars synthesized a series of such push–pull compounds and discussed the resulting red-shifted absorption maxima of hemicyanine dyes due to their extended conjugated electronic systems that allowed energy-reducing resonance formulas. This fundamental contribution was published back-to-back with another paper that added theoretical calculations to this phenomenon [40].

The replacement of the cyclohexenyl ring of retinal by p-amino substituted phenyl rings yielded, when assembled with bO, a λ^{a}_{max} of 615 nm (either mono- or dimethyl amino substituents), and generated also other microbial rhodopsins, strongly red-shifted pigments [36]. In some applications, these compounds were fine-tuned for fitting into the binding site by addition of two ortho-placed methyl groups (thereby, the ring moiety is described as a 2,6-dimethyl-4-methyl amino phenyl ring; these compounds were then coined as MMAR) [41, 42]. Not only yielded the MMARs red-shifted absorptions upon assembly with bO, but, more importantly, they showed a strong, extremely red-shifted fluorescence (in contrast to bR that is nearly void of any fluorescence). A detailed study of MMAR-assembled proteorhodopsin documented the interesting properties of these MMAR-type chromophores [43]. In fact, the strong red shift in both absorption and fluorescence of an MMAR-substituted proton pump from *H. sodomense* allows its use as a voltage sensor and makes these pigments promising tools in neuro-biological applications [44]. The concept of synthesizing push–pull systems was optimized by Liu and coworkers who replaced the cyclohexenyl ring of retinal by an azulenic ring system, and in addition, they replaced the methyl group at position 13 by a trifluoromethyl group [45]. These changes clearly revealed the diverse forces that the protein environment exerts on the chromophore properties [46].

Merocyanines carrying an electron-donating heteroatom on one end, e.g., a nitrogen atom, and an electron-withdrawing heteroatom on the other (consider an aldehyde group) [47], are attractive model compounds to probe the impact of the protein environment on the spectral properties of the retinal chromophore in bR. With their hetero-aromatic nitrogen-containing ring and the carbonyl group at either end, the delocalization of the electronic

structure is much more pronounced than in the retinal. Such compounds would become hemicyanines upon conversion of their electron-withdrawing carbonyl group into a protonated Schiff base (PSB), and already in solution would mimic the PSB formation taking place upon binding of such compounds to bO. Thereby, one can probe the composite effects of the protein on the absorption and photochemical properties upon chromophore incorporation. In addition, this study also aims to answer the challenging question, 'to what extent does a fully conjugated polyene system still undergo the chromophore-characteristic photochemistry?'.

Here, we continue a former study presented in a short communication [35] and report the complete information on the synthesis of a series of 11 merocyanine dyes (Fig. 1) and their interactions with the apoprotein bO which result in remarkably bathochromically shifted absorption maxima of the formed hemicyanines. Interestingly, the structural features of these merocyanines reported in above-cited short note had stimulated research to employ this

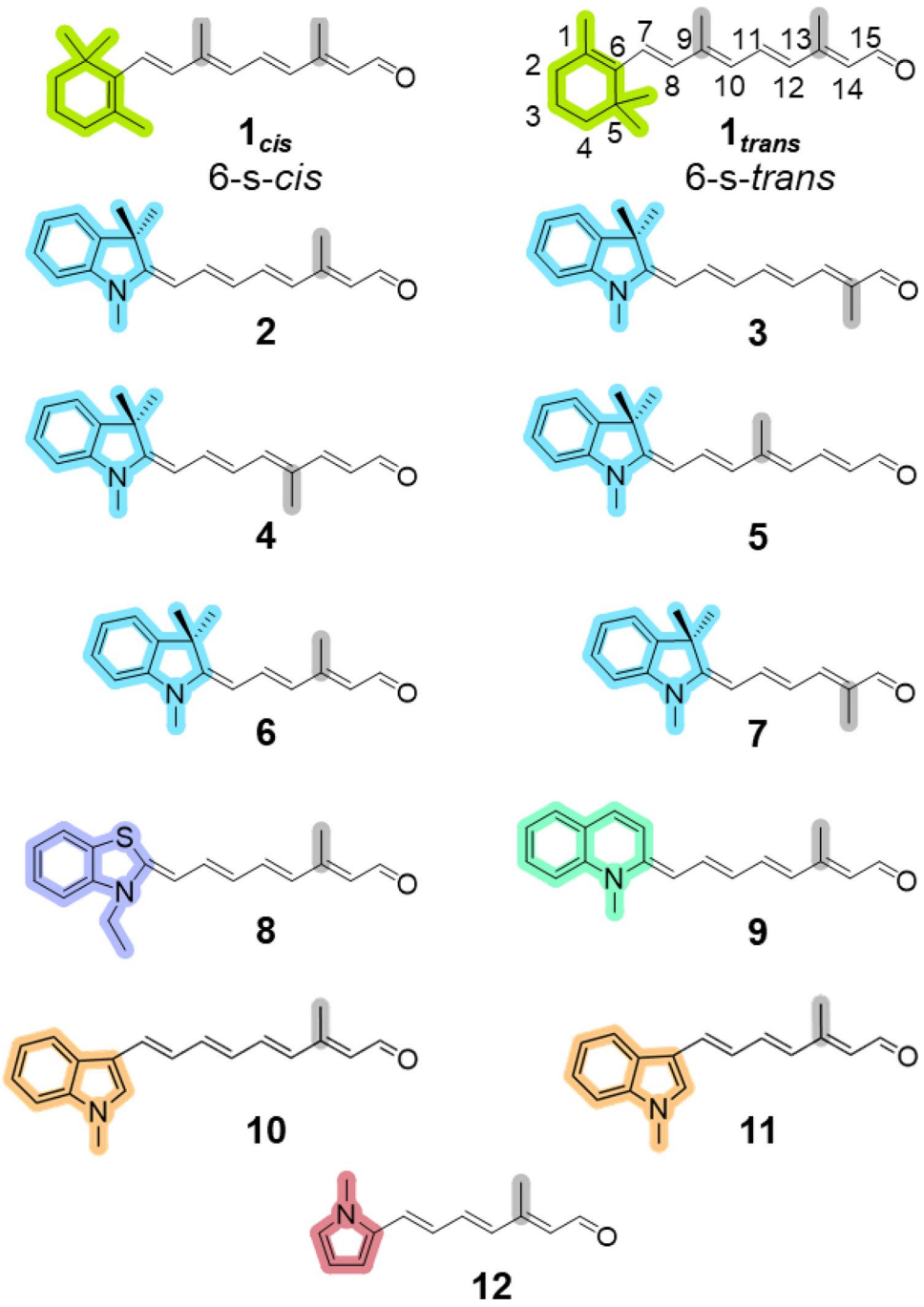

Fig. 1 Structural formulae of retinal derivatives **1**–**12** in the aldehyde form. Different terminal rings are highlighted in color. The position of the methyl group(s) along the polyene chain is shown in gray. The conventional numbering for retinal carbon atoms is shown for $\mathbf{1}_{trans}$

compound class for microbiological investigation. Herwig et al. [48] had incorporated merocyanine **2** (see Fig. 1) into Archaerhodo-psin-3 (Arch), a light-driven proton pump from *H. sodomense* (see above-cited work with MMAR retinal analogues). The novel Arch showed strong fluorescence (brightness 8.5-fold that one from the native Arch) and an emission maximum ca. 200 nm red-shifted to the native pigment. The authors succeeded to incorporate this cyanine-Arch into the membrane of living *E. coli* cells and demonstrated the higher visibility in microscopic applications.

The retinal-like merocyanines depicted in Fig. 1 were designed with polyene chains in length of three or four double bonds and carry ring substituents of 2,3-dihydro-1,3,3-trimethylindol-2-ylidene, 2,3-dihydro-3-ethylbenzothiazol-2-ylidene, 1-methyl-quinolin-2(1*H*)-ylidene, *N*-methyl-3-indolyl, and *N*-methyl-2-pyrrolyl groups with a terminal aldehyde end group to allow the formation of a PSB with the lysine of bO. The results from the protein–chromophore interactions are compared to the spectroscopic properties of these compounds after conversion into PSBs in organic solvents. The experimental results are complemented by quantum chemical simulations of the excitation energies of the retinal analogues in the gas phase, solution, and in the protein environment. The spectral tuning of the analogue bRs is revealed by combined quantum mechanics/molecular mechanics (QM/MM) simulations. The comparison of the changes in the electronic structure of the chromophore upon excitation and the electrostatic potentials imposed by the protein on the chromophore help to understand the spectral shifts.

2 Materials and methods

2.1 Chemical section

Triethylphosphite and chloroacetonitrile were purchased from Aldrich, and 3,3-dimethyl-acrylonitrile was purchased from Merck Schuchard. Fischer aldehyde **13** [2,3-dihydro-1,3,3-trimethylindol-2-ylidene-acetaldehyde] and phosphoniumacetal **26** were generously provided by BASF AG Ludwigshafen. Fischer aldehyde **13** was recrystallized from Ligroin before use. Silicagel 60 for chromatography was from Merck Schuchard. Solvents were dried and purified according to the standard procedures. All other reagents were of analytical grade.

Compounds **2**–**12**—out of which compounds **2**–**7** had been briefly described in the former publication [35]—were characterized by ^{1}H-NMR, ^{13}C-NMR, IR, UV/Vis, high-resolution mass spectroscopy, or elementary analysis (see Supplementary Material; for an assignment of all compound numbers to chemical structures, see Figs. 1 and 2). The spectroscopic data were in full accordance with the expected structures. For compounds **2**–**7**, the same starting material ("Fischer-Aldehyde", 2,3-dihydro-1,3,3-trimethylindol-2-ylidene-acetaldehyde, **13**) was employed. Polyene chain extension followed the established Wittig–Horner route. Aldehydes were condensed with ylids from phosphonates of different chain lengths and substitution patterns that carry a nitrile end group. The nitrile end group of the new reaction product was then reduced to new aldehyde groups by DIBAH. We describe here in all detail only the synthesis of compound **2** (for the synthesis of all other merocyanines and spectroscopic and analytical details, see Supplementary Material).

2.2 Synthesis of trimethylindolenine retinal derivatives 2–7

(a) 4-(2,3-Dihydro-1,3,3-trimethyl-indol-2-ylidene)-but-2-enenitrile 14

To a suspension of 7.2 g (0.3 mol) sodium hydride (80% in paraffin) in 70 mL tetrahydrofurane (THF), a solution of 39.6 g diethyl (cyanomethyl)phosphonate in 40 mL THF was added dropwise at 0 °C under nitrogen. For the formation of the ylide, the solution was refluxed for 30 min. After cooling to room temperature, 15.0 g (75 mmol) of Fischer aldehyde **13** dissolved in 70 mL THF were introduced dropwise under nitrogen. This solution was again refluxed for 1 h. After cooling, 70 mL brine was added, followed by extraction with dichloromethane and drying of the combined organic phases. After evaporation and column chromatography (silica gel, dichloromethane/diethyl ether 1:1) 12.9 g (58 mmol = 77%) of nitrile **14** was obtained (mp 90 °C). M (calculated): 224.1313, M (found): 224.1297 ± 0.0023.

(b) 4-(2,3-Dihydro-1,3,3-trimethyl-indol-2-ylidene)-2-butenal 15

12.0 g (53 mmol) nitrile **14** dissolved in 50 mL dichloromethane were allowed to react with 160 mL of 1 M DIBAH in dichloromethane for 2 h under nitrogen at room temperature. After hydrolysis with wet silica gel, extraction, drying, and solvent evaporation, column chromatography (dichloromethane/diethylether 1:1) yielded 6.7 g (29 mmol = 55%) of aldehyde **15** (mp 131 °C).

(c) 8-(2,3-Dihydro-1,3,3-trimethyl-1H-indol-2-ylidene)-3-methyl-2,4,6-octatrienal 2

To form the ylide of diethyl (3-cyano-2-methyl-2-propenyl)phosphonate, 7.2 g (33 mmol) phosphonate in 30 mL THF were added dropwise to 1.1 g (45 mmol) of sodium hydride (80% in paraffin) in 30 mL THF at 0 °C under

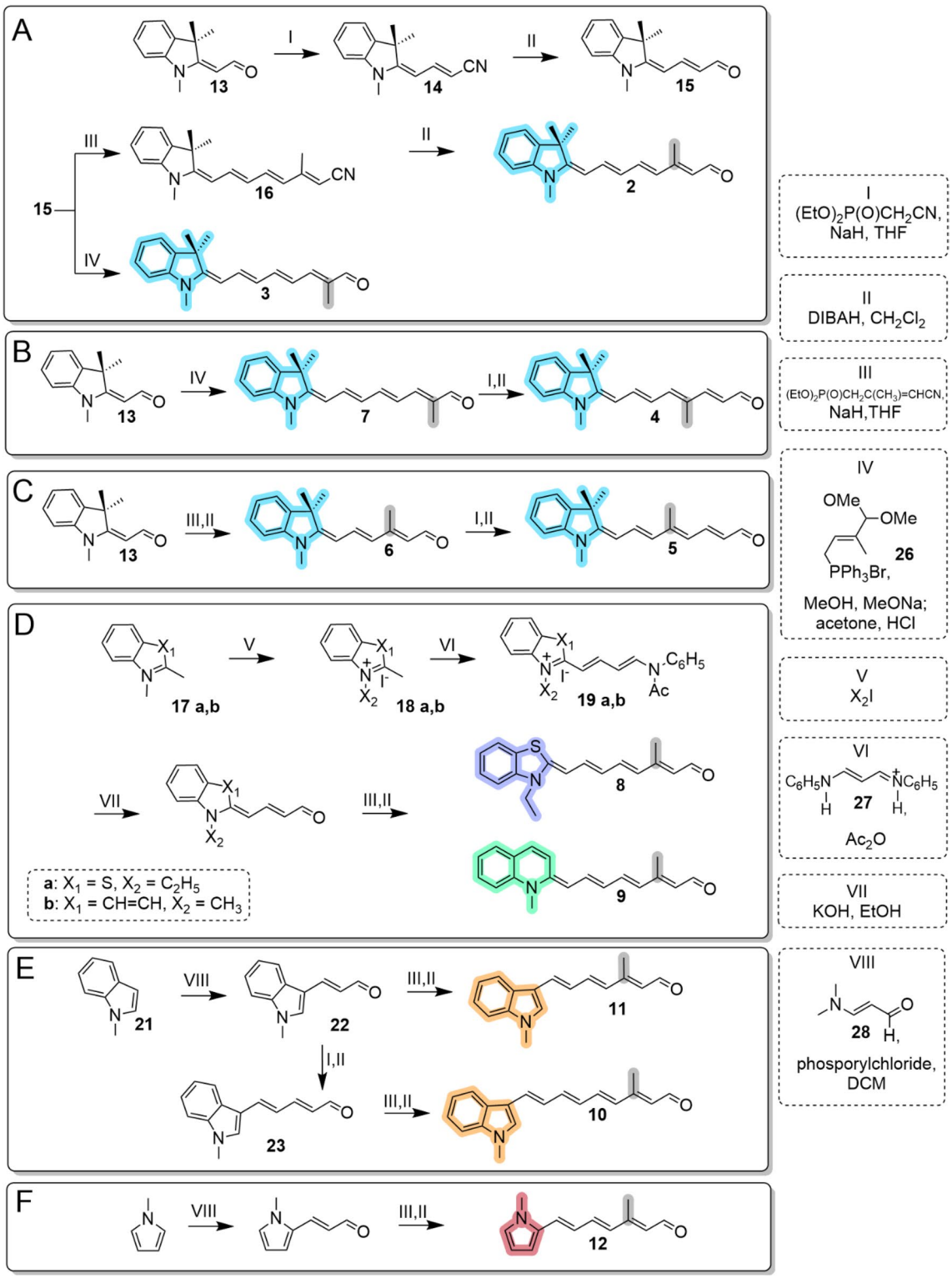

Fig. 2 Schematic presentation of synthesis of novel merocyanines A) **2** and **3**, B) **4** and **7**, C) **5** and **6**, D) **8** and **9**, E) **10** and **11**, and F) **12**. Right hand panel lists reagents and molecules involved in the syntheses

nitrogen. This solution was refluxed for 30 min. After cooling, 2.5 g (11 mmol) of aldehyde **15** in 30 mL THF were added. This solution was again refluxed for 15 min. After conventional work-up according to the procedure (**1a**) and column chromatography (dichloromethane/diethyl ether 1:1), 2.2 g (8 mmol = 69%) of nitrile **16** were obtained (mp 126 °C). Reduction of nitrile **16** with DIBAH was identical to procedure (**1b**). The reaction between 2.0 g (7 mmol) of compound **16** and 20 mL DIBAH (1 M in dichloromethane) yielded 1.2 g (4 mmol = 57%) of **2** (mp 99 °C).

2.3 Synthesis of protonated Schiff bases from aldehydes 1–12

To ethanolic solutions of aldehydes **1**–**12** (volumes of 50 mL, adjusted absorption of 1.0 in a 1 cm path length cuvette), 200 µL n-butylamine were added in the dark and the resulting mixture was allowed to react for ca. 15 min. After this incubation, UV–Vis absorption spectra were recorded from aliquots of these solutions. Protonation of the Schiff base (SB) solutions generating the protonated Schiff bases (PSB) was performed by addition of 200 µL of concentrated hydrochloric acid. UV–Vis absorption spectra were immediately measured after the addition. The di-cation of the SB of compound **9** (protonation of the chinolin nitrogen atom) was obtained after further addition of 50 µL of concentrated hydrochloric acid (Fig. 3).

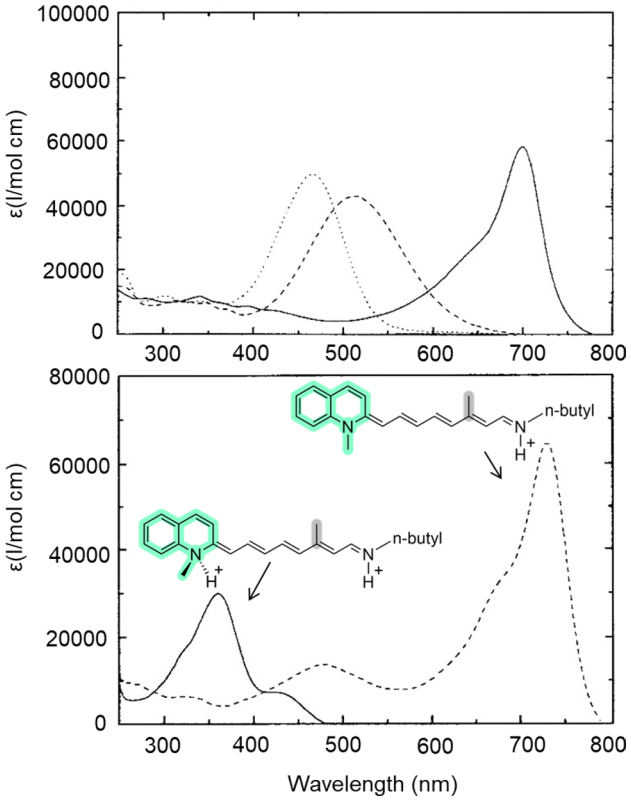

Fig. 3 Absorption spectra of molecule **8** with the free aldehyde (dashed), SB (dotted), and PSB (solid line) forms (top panel). Absorption spectra of molecule **9** with the PSB form (dashed) and the di-protonated SB (solid line, bottom panel)

2.4 Microbiological and biochemical section

2.4.1 Formation of chromoproteins and pH-dependence of fully reconstituted hemicyanine-containing bRs

The apoprotein bO was prepared from the retinal-deficient *H. salinarum* strain JW5, following the standard protocols [35]. Chromoproteins were reconstituted at ambient temperatures by incubating bO (10–15 µM in a volume of 3 mL) in the dark with the newly synthesized merocyanines. The aldehydes were added in highly concentrated form (vol. < 10 µL), dissolved in ethanol or isopropanol. In the case of compounds **5**, **8**, and **9** which showed only low solubility in alcohols, solutions in DMSO were applied. The final chromoprotein concentration was between 5 and 10 µM. For experiments investigating the pH-dependence of the absorption spectra, sodium phosphate buffers with pH values of 9, 7.5, 6, and 4 were prepared. 50 µL of fully reconstituted chromoproteins were diluted into 700 µL of the buffer, such that absorbances of 0.1–0.2 at their maximum resulted. These solutions were directly measured in the UV–Vis photometer.

2.4.2 Irradiation protocol

Samples of reconstituted bRs were irradiated with light from a slide projector bulb (250 W), equipped with interference or cut-off filters, according to the required wavelengths. The samples were placed in front of the projector at a distance of ca. 25 cm.

2.4.3 Fluorescence measurements

Fluorescence measurements were performed with a Spex-Fluorolog. The samples had an absorption of 0.05 at the excitation wavelength.

2.5 Computational methods

2.5.1 Solution models

The aldehyde, SB, and PSB structures of the retinal analogues **1**–**12** were optimized in the gas phase and in solution using B3LYP/cc-pVDZ with Grimme's D3 (GD3) dispersion corrections [49–52]. The calculations in solution employed a polarized continuum model (PCM) with

ethanol as the solvent. The minimum structure was confirmed by a frequency calculation where no imaginary frequencies were present. The C_6–C_7 single bond (Fig. 1) connecting the polyene moiety with the cyclohexenyl ring can assume two conformations. Therefore, we computed both the 6-s-*cis* and 6-s-*trans* conformations of retinal and these will be referred to as $\mathbf{1}_{cis}$ and $\mathbf{1}_{trans}$ (Fig. 1), respectively. The aldehyde, SB, and PSB models of $\mathbf{1}_{cis}$ and $\mathbf{1}_{trans}$ are shown in the SI Fig. S1. Similar to retinal, the compounds **10**, **11,** and **12** also had a single bond between the polyene chain and the ring. Hence, two models were generated to determine which would be lower in energy. The heterocycles were rotated by 180° around the polyene chain (Fig. S2) and the relative energetics of s-*cis* and s-*trans* compared (Table S1).

To reduce the computational cost, the n-butyl group was replaced as described below. For the SB models, either a hydrogen (SB_H) or a methyl group (SB_{Me}) was introduced at the SB nitrogen. Two substituents for the iminium nitrogen were considered for the PSB: (i) a hydrogen (PSB_H) and (ii) a methyl group (PSB_{Me}). In the case of the PSB_{Me} models, the effect of the Cl^- counterion was evaluated (PSB_{Me+Cl-}). The Cl^- ion was added in the plane of the polyene chain of the PSB_{Me} models with a distance of 3.0 Å from the SB nitrogen and 3.0 Å from the carbon of the methyl substituent (Fig. S3). This procedure was systematically completed for each derivative. The aldehyde, SB, and PSB_{Me+Cl-} models were neutral, whereas PSB_H and PSB_{Me} had a positive charge. The geometry optimizations were completed in Gaussian 09 [53].

2.6 Hybrid QM/MM models

Retinal ($\mathbf{1}_{trans}$) and molecule **2** were described in the bR protein environment using the hybrid QM/MM method (Fig. 4). Compound **2** was selected, because it was among the most red-shifted derivatives and comparable to retinal in terms of the length of the polyene chain. Due to the high computational cost of studying all the analogues, we limited our QM/MM calculations to a comparison of **1** and **2** in bR. The bR models were generated from the high-resolution crystal structure of bR (PDB ID 7Z09) [22]. Hydrogens were added using the *tleap* program from the AMBER 16 package [54, 55]. The counterions, Asp85 and Asp212, were not protonated (Fig. 4), and the remaining titratable residues were set to the default value at pH 7. The parameters for retinal and **2** were determined via *antechamber* in AMBER 16 [54, 55]. The waters present in the crystal structure were retained for the simulations. The system was pre-optimized via the steepest descent algorithm for 250 steps followed by 750 steps with the conjugate gradient algorithm. Subsequently, the system was further minimized using the hybrid QM/MM approach using the semi-empirical DFTB [56] method for the QM part. The QM region contained the retinal molecule and the side chain of Lys216 where the partitioning between the QM and MM regions was made between the Cα and Cβ. The cut between the Cα and Cβ was chosen

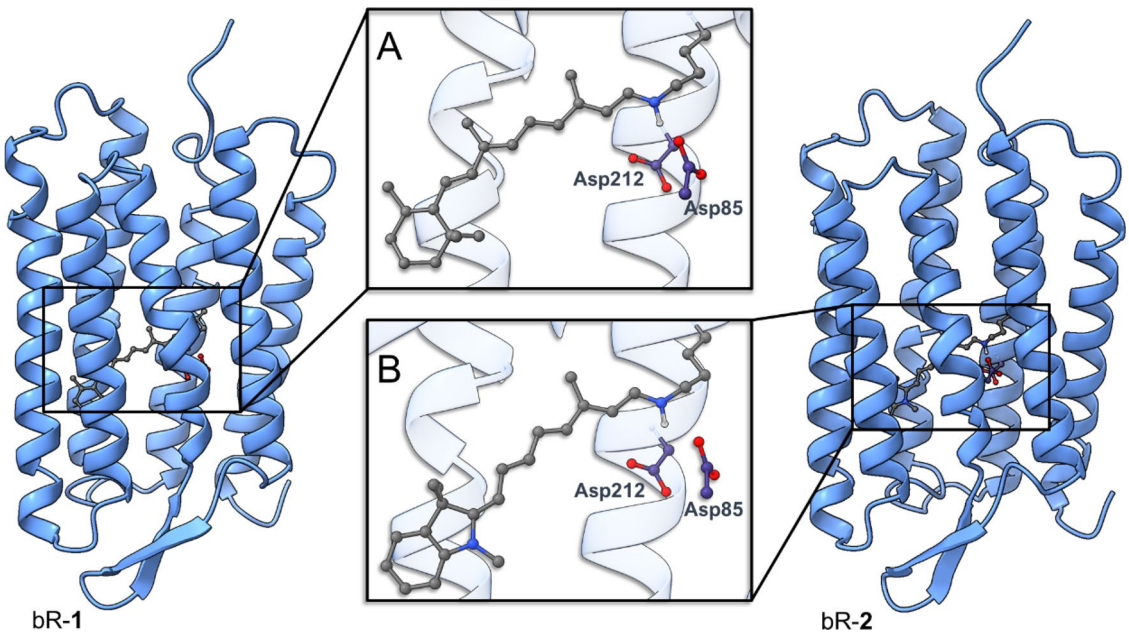

Fig. 4 QM/MM optimized models generated from PDB ID: 7Z09 where the chromophore is A) $\mathbf{1}_{trans}$ and B) **2**. The counterions, Asp85 and Asp212, are shown in purple

based on our previous studies of retinal proteins [57–59]. The resulting structure was used for the QM/MM optimization using the B3LYP functional with cc-pVDZ basis set as part of the QM region. In addition, dispersion correction [52] with Becke–Johnson damping (D3BJ) [60] was applied to B3LYP. The L-BFGS [61] optimizer was used for the optimization. In our setup, all residues within 5 Å of the chromophore were allowed to freely move throughout the optimization except for their backbone atoms. All protein residues and the backbone of Lys216 were included in the MM region and treated with the ff14sb force field [62]. The DFTB calculations were carried out in AMBER 16. The QM/MM optimizations of bR-**1** and bR-**2** were performed in Orca.

2.7 Calculation of vertical excitation energies

The vertical excitation energies for each of the retinal derivatives were carried out in both the gas phase and solution for all models under consideration. The retinal derivatives were optimized in the ground state prior to the excited-state calculations. We used time-dependent density functional theory (TD-DFT) with the TD-CAM-B3LYP [63] functional with the cc-pVDZ [51] basis set. In addition, the algebraic-diagrammatic correction scheme to the second-order ADC(2) [64, 65] was applied with the same basis cc-pVDZ. For the TD-DFT calculations in ethanol, a PCM solvent model was used and for the ADC(2) calculations, a Conductor-like Screening Model (COSMO) [66, 67] was used. Three excited states were calculated for each model and the corresponding oscillator strengths were used to determine the bright state. The root-mean-square error (RMSE) between the experimental and the calculated vertical excitation energies was computed and the equation is described in Fig. S6. The TD-CAM-B3LYP calculations were completed in Gaussian 09 and the ADC(2) calculations were completed in Turbomole version 7.3 [68, 69].

3 Results and discussion

A series of merocyanine dyes were synthesized and employed as chromophores in bR (Fig. 1). Instead of the cyclohexene ring that retinal possesses, the ring substituents of the derivatives were varied into *N*-methyl-3,3-dimethylindolylidene (**2**–**7**), *N*-ethyl-benzthiazolylidene (**8**), *N*-methyl-1,2-dihydro-chinolin-2-ylidene (**9**), *N*-methyl-3-indolyl (**10**, **11**), and *N*-methyl-2-pyrrolyl groups (**12**) (Figs. 1, 2). Methyl substitution of the ring nitrogen atoms was required in all cases to prevent side reactions of the heteroatoms during the synthesis. Due to the low reactivity of some of the starting materials, e.g., **13** (Fig. 2), the syntheses turned out to be difficult and demanded variation of the commonly used Wittig–Horner route (Fig. 2) [35].

3.1 Absorbances of retinal derivatives

As expected from their merocyanine structure [35], the absorbances of the new compounds in organic solvents are all red-shifted compared to that of retinal (Table 1). The most bathochromic absorption is found for compound **9** (λ^a_{max}: 540 nm, cf. λ^a_{max} of retinal: 380 nm). The red-shifted

Table 1 Spectral properties (λ^a_{max} and ε_{max}) of free aldehydes, Schiff bases (SB), and protonated SB (PSB) all measured in ethanol

	Aldehyde		SB	PSB	bR		OS (cm^{-1})
	λ^a_{max} (nm)	Log ε	λ^a_{max} (nm)	λ^a_{max} (nm)	λ^a_{max} (nm)	Log ε	
1	381	4.60	357	440	570	4.80	5183
2	487	4.63	448	666	755	5.43	1770
3	482	4.65	465	657	700	5.23	935
4	490	4.75	452	657	698	~5.36[a]	894
5	491	4.61	453	665	711[b]	–[c]	973
6	463	4.46	420	578	610	~5.08	908
7	456	4.78	422	567	–[c]	–	–
8	511	4.58	465	701	736	5.09	678
9	540	4.68	479	730	766	5.19	644
10	441	4.55	411	533	–[c]	–	–
11	421	4.32	390	515	–[c]	–	–
12	420	4.42	391	504	–[c]	–	–

The bR values are reported from the incubation of bO with merocyanines **2–12**. The OS is listed in the last column in cm^{-1}

[a]There are two isomers present with partially overlapping absorption bands

[b]No complete reconstitution between **5** and bO

[c]No covalent chromophore protein binding (for details, see "Results" section)

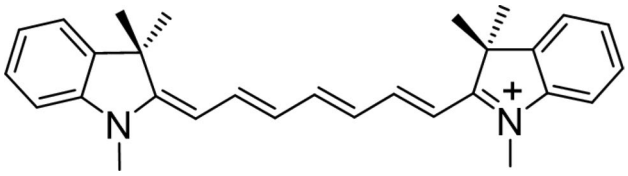

Scheme 1 A symmetrical cyanine compound where the double and single bonds are nearly identical in length [71]

absorption maxima can be explained from a strong contribution of the aromatic π-system of the nitrogen-based ring system to the polyene chain absorption. The geometry optimizations of the retinal analogues with DFT show that the ring component and the polyene chain of the retinal analogues are planar, which allows for excellent π-conjugation in these molecules.

While the cyanines studied here exhibit strongly bathochromic absorption maxima, there are a few anomalies to point out. The red shift between the SBs and PSBs of **10**–**12** is not as dramatic as the other hemicyanines. This moderate red shift can be understood from the structure of these compounds that do not show cyanine-like properties per se but exhibit a more polyene-like character. This becomes obvious from a comparison of the absorption maxima upon extending the polyene chain by one double bond. The additional double bond (from **6** to **2** or from **7** to **3**) leads to a shift of the absorption maximum by ~ 90 nm (578 to 666 nm, $\Delta = 2286$ cm^{-1} and 567 to 657 nm, $\Delta = 2416$ cm^{-1}), respectively. On the other hand, the extension of the side chain by one double bond (as seen in **11** to **10**) adds only 18 nm to the position of the absorption maximum (515–533 nm, $\Delta = 656$ cm^{-1}).

For further discussion, we wish to differentiate between a 'polyene-like' and a 'cyanine-like' electronic configuration in this study, as neither retinal nor the merocyanines match exactly the definition of their compound class with respect to their electron distribution. Considering the crystal structure of retinal [70], one finds with respect to bond lengths a clear alternation of single and double bonds (C7–C8: 1.315 Å, C8–C9 Å: 1.467 Å, C13–C14: 1.344 Å, C14–C15: 1.455 Å. In contrast, the central bonds in a fully symmetric cyanine (Scheme 1) are indistinguishable in length, i.e., the single and double bonds have become equal in length [7].

In an early study, Tavan et al. calculated, based on the crystal structure of retinal, the SB of retinal and the effect of the retinal–SB protonation, aiming to understand the effect of a positive charge in the vicinity of the 13–14 bond [37]. This study demonstrates the effect of protonation: C7–C8: 1.346 Å, C8–C9 Å: 1.471 Å, C13–C14: 1.408 Å, C14–C15: 1.400 Å, i.e., C13–C14 and C14–C15 bonds become of equal length.

In contrast, the incorporation of the novel merocyanine compounds in the bO results in much smaller OS, compared to the native retinal chromophore. The top 3 most red-shifted PSBs in solution were **9**, **8**, and **2** where the absorption maxima were 730, 701, and 666 nm, respectively. In bR, the most bathochromically shifted merocyanines were: **9**, **2**, and **8**, where the absorption maxima were 766, 755, and 736 nm, respectively. The incorporation of merocyanines **9**, **2**, and **8** into bR yielded absorption maxima which are even more red-shifted than a recently discovered neorhodopsin (NeoR, $\lambda^{a}_{max} = 690$ nm) [59]. It is clearly an intrinsic effect of the altered chromophores, since NeoR carries a canonical retinal chromophore **1**. These three derivatives share two common features, namely the position of the methyl sidechain at the retinal 13 position and the length of the polyene chain of 8 carbons. Interestingly, the heterocycles for **9**, **2**, and **8** are distinct, perhaps indicating that the key to the red shift is not dependent on the type of ring system employed. The red shift clearly results from the ability to shift the charge from the iminium nitrogen farther across the polyene chain than in retinal which is provided by the additional nitrogen in the ring systems.

The effect of the methyl group position can be extracted from the series of derivatives **3**, **4**, and **5**. They have the same heterocycle as in **2** and also an 8-carbon length polyene chain. The only difference between **2** and the structures of **3, 4**, and **5** is the position of the methyl group, yet **2** has a red shift of more than 40 nm compared to them. This indicates that the position of the methyl group is a strong contributor to the extent of the red shift—at least among this group of merocyanines. It can be explained using resonance structures where the positive charge is delocalized along the polyene chain (Scheme 2) [8]. The ground state electronic structure is described by resonance structure I, while the excited-state electronic structure is a combination of resonance structures I–VII. The resonance structures have the positive charge on the carbon atom with an uneven number. If a methyl group is introduced in such a position, it is lowering the excited-state energy and therefore leading to a red shift. In bR-**5**, the methyl group is at position 11, and in **3,** it is at position 14 (referring to retinal numbering, Fig. 1). This indicates that the position of the methyl group is a strong contributor to the extent of the red shift—at least among this group of merocyanines.

3.2 Formation of protonated Schiff bases

The conversion of the aldehyde into a SB in organic solvents upon addition of n-butylamine, followed by protonation, could be accomplished with all compounds and led to a strong bathochromic shift of the absorption (Table 1). The hemicyanine character of the PSB, which formally allows the positive charge to move along the entire polyene chain

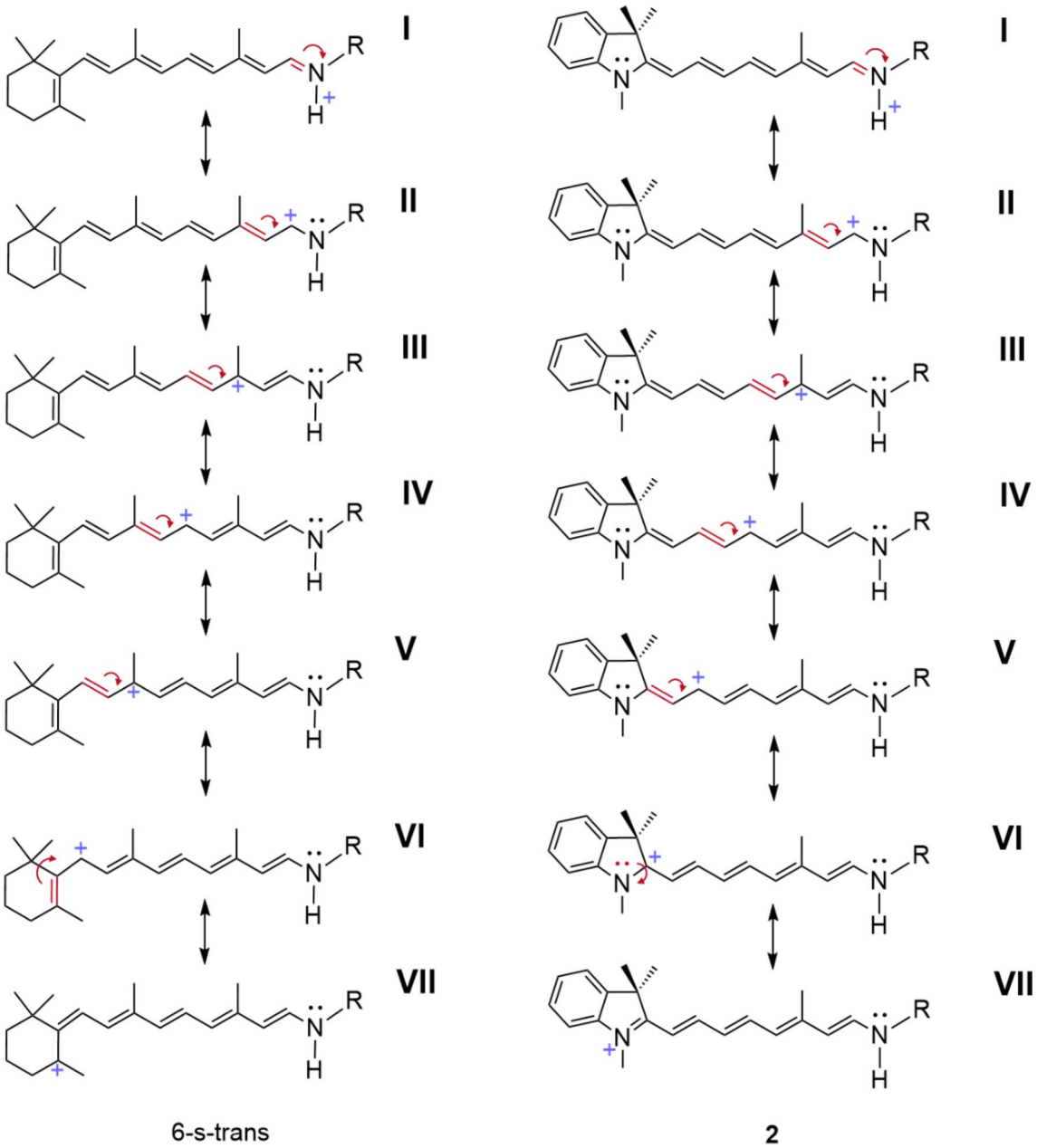

Scheme 2 Resonance formulas for the PSBs of (left) 6-s-*trans* retinal **1** and of (right) molecule **2**

into the hetero-aromatic end group, is evident from the very narrow absorption bands with half-bandwidths of 1000 cm^{-1} (Fig. 3, top), except for compounds **10**–**12**. For these latter three derivatives, broad absorption bands (half bandwidth around 4000–5000 cm^{-1}) are obtained in the PSB form. The increased width indicates that a more polyene-like electronic structure is present. This is due to a structural feature of compounds **10**–**12** where the aromatic ring is connected to the polyene by a single bond, instead of a double bond. The single bond makes an involvement of the hetero-aromatic nitrogen atom in the conjugated system less efficient and thereby reduces the hemicyanine character for this compound. The higher flexibility in the rotation of the single bond in comparison to the double bond leads to a greater range of twisted structures leading to a broader absorption band.

Even for the merocyanines with only three double bonds in the polyene chain (**6**, **7**, **11**, **12**), the bathochromic shift upon PSB formation is larger than that of retinal (3520 cm^{-1}). Except for **10**, which exhibits a relatively moderate absorption shift upon PSB formation (3915 cm^{-1}), the merocyanines with four double bonds all showed red

shifts around 5000 cm^{-1}. Ongoing acidification introduced a second positive charge on compound **9** by the protonation of the chinolin nitrogen, leading to a hypsochromic shift of the PSB absorption from λ^a_{max} 730 to 360 nm (shown for the PSB of **9**, Fig. 3, bottom). This conversion was found to be reversible after raising the pH, indicating that the change of absorbance is not due to decomposition of the compounds under the experimental conditions.

As can be seen from the example of compound **9** in Fig. 3, the PSB form of the merocyanines (compound **2**–**9**) exhibits absorption bands quite similar in spectral position (Table 1) and shape to the form reconstituted in bR (see next paragraph). Some of these compounds, already in the PSB form, present vibrational (progression) bands with a high-energy shoulder, typical for cyanines and hemicyanines [72–79]. This indicates that in this class of compounds, most of the electronic arrangement which retinal experiences upon covalent binding to the protein is inherently present when the PSBs are formed in organic solvents [39, 40].

3.3 Reconstitution of analogue bRs

Analogue bRs could be formed with most of the merocyanines (**2**–**6**, **8**, **9**) and showed strongly red-shifted narrow absorption bands. A more complex assembly process was found for compound **10** that formed a pigment, however, with remarkably different spectral features than compounds **2**–**6**, **8**, **9** (see below). The time period for full reconstitution (at ambient temperature) varied from a few minutes (*e.g.,* **8**, Fig. 5a) up to several hours. The assembly of compound **2**, which requires several hours for completion, has already been shown [35]. Compound **6** (with only three double bonds in the polyene chain) led to the formation of a pigment absorbing at 610 nm. The "full-length" compounds (**2**–**5**, **8**, **9**) reconstituted with bR had strongly red-shifted absorption maxima spanning the spectral range from 700 nm (**3**–**5**) up to 766 nm (**9**).

The most bathochromic absorption maxima are found for compounds bR-**2** (λ^a_{max} = 755 nm) and bR-**9** (λ^a_{max} = 766 nm). These compounds have four double bonds and the methyl group at the same position, but there is a difference in the ring end group. The dimethyl group at carbon position 3 of the indolenine ring of **2** may cause a steric hindrance, but also the extension of the conjugation to the additional double bond in the quinoline ring of **9** might be the reason of the slightly further red-shifted absorption maximum of bR-**9** by 11 nm. In bR-**3**, the absorption maximum is 700 nm which is strongly blue-shifted to that of bR-**2** (λ^a_{max}= 755 nm). The difference between bR-**3** and bR-**2** is in the placement of the methyl group along the polyene chain. As described above, this can be rationalized on the basis of resonance structures in Scheme 2. In bR-**3,** the side chain methyl is located at position 14, while for bR-**2,** the methyl side chain is located at the equivalent position of retinal, position 13 (for retinal numbering, see Fig. 1).

As expected for hemicyanines, the absorption bands of all merocyanine-reconstituted bRs exhibit very narrow half-bandwidths and large extinction coefficients (Table 1). In the case of compound **4**, two isomers (or two different conformations) formed during the reconstitution, although, isomerically pure material was initially used for the assembly [80]. This became obvious from a shoulder of the absorption band at its long-wavelength tail (λ^a_{max}= 741 nm) [35]. Also, for compound **5**, two conformers or isomers have apparently formed, since a shoulder at the long-wavelength tail (maximal absorbance around 740 nm) can be observed [35, 80]. For compound **5**, no complete reconstitution could be accomplished, even when a large excess of aldehyde over apoprotein was applied. This became apparent when a 'fully' assembled bR-**5** sample was incubated with all-*trans* retinal yielding the formation of native bR.

Here, it should be pointed out that there are examples of opsin-embedded cyanine analogues of retinal that are red-shifted but lack the characteristic narrowly shaped

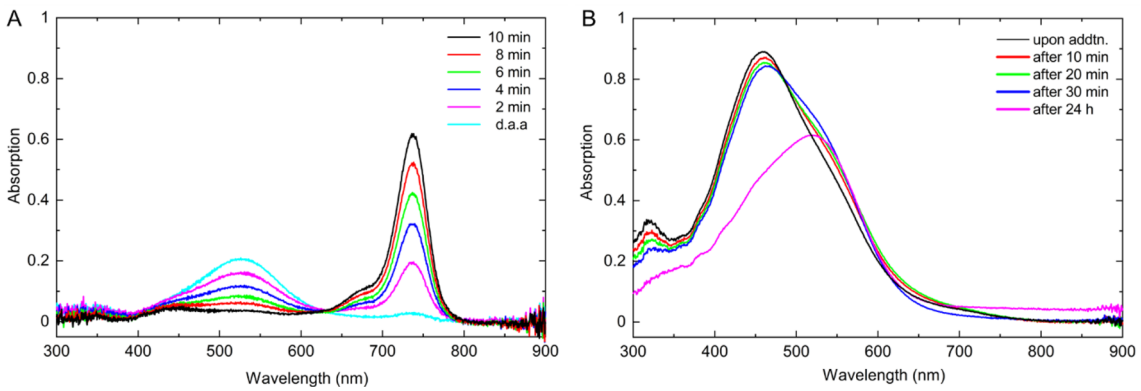

Fig. 5 Reconstitution of A) merocyanine **8** in bR and B) incubation of bO and merocyanine **10**

absorption band. An interesting case is the aforementioned MMAR incorporated into proteorhodopsin that yields a strongly red-shifted absorption band (around 700 nm), and a strong fluorescence emission around 840 nm [42, 43].

Reconstitution failed with compounds **7**, **11,** and **12.** These compounds have short polyene chains in common and this might cause a steric hindrance by the ring moiety preventing the aldehyde group from penetrating deeply enough into the protein cleft to accomplish covalent bond formation with the lysine residue. Although incubation of bO with **11** and **12** started with formation of a shallow absorption band around 600 nm, after 2 days, the band nearly vanished, and a slight tailing was found at the long-wavelength side of the absorption band of the aldehyde. The length of the polyene is not the only factor for covalent binding. Compound **6** has the same length as **7,** but the methyl group is further away from the aldehyde in the former which seems to impact the incorporation in the protein-binding pocket.

Merocyanine **10** carries a polyene chain with the same length as retinal, and thus was expected to form a stable bR analogue. The reconstitution behavior of this compound indeed gave evidence for a specific interaction with the protein. Within 30 min of incubation with bO, a very broad absorption band around 530 nm formed, with an isosbestic point at ca. 485 nm (Fig. 5b). However, the relatively small shift of the absorption maximum in the protein as well as the small shift between the absorption of the free aldehyde and the PSB (3914 cm^{-1}, see Table 1) point to a more polyene-like electronic structure of this compound. This might also explain the different interaction with the protein compared to the other merocyanines. Note that **10** and also **11** carry an indolyl ring structure yielding an aromatic ring system, whereas compounds **2**–**7** carry 2,3-dihydro-indolyl rings that are linked in position 2 of the indolyl ring. The proximity of the polyene chain to the indole-nitrogen for **2**–**7** might improve the conjugation of the entire compound. It might also be kept in mind that only compounds **10** and **11** carry their ring substituents 'below' the polyene chain plane, whereas all other compounds carry their ring substituents 'above' the polyene chain. In addition, the ring moiety in compounds **10**–**12** is connected to the polyene chain by an additional single bond akin the bond structure in **1**, whereas in all other compounds, the ring structure is part of the polyene chain.

Considering the assembly experiments, note that compounds **3**, **4**, and **7**, and also **12** carry the methyl group substitution in the polyene chain at the 'wrong' position potentially causing an additional barrier for SB formation with the protein. Compounds **3** and **4** carry their methyl group at retinal positions 12 and 14, respectively, still allowing bR formation upon assembly, whereas for **7,** the shortened side chain together with the 'wrong' position of the methyl group now inhibits bR formation. The 'misplaced' methyl groups (**3**, **4**) results in less red-shifted absorption maxima for their bRs compared with the correctly placed methyl group in **2** (λ^a_{max} bR-**2**: 755 nm, bR-**3**: 700 nm, and bR-**4**: 698 nm); note that positioning the methyl group at positions 12 or 14 yields nearly the same reduction of the absorption maximum compared with **2**. Clearly, the embedding of **3** and **4** into the bO-binding site requires a conformational adaptation of the amino acid side chains to allow additional space for the methyl groups. Proof is given by comparison of the CD-spectra. Previous work [35] demonstrated a very shallow negative lobe in the CD-spectrum of bR-**3** in relation to those of native bR and bR-**2**. The latter two bRs both show very similar CD-spectra with a positive lobe in the region of the short-wavelength flank of the absorption band, an inflection point at the absorption maximum, and a negative lobe in the region of the long-wavelength flank.

3.4 Quantum chemical calculations

The remarkable absorption properties of the novel retinal-like compounds in ethanol and even more so after assembly with bO called for quantum chemical calculations to provide a detailed understanding of the spectral properties. In the following, we describe the computational results in the gas phase, solution, and in the protein environment.

3.4.1 Simulations in the gas phase and in solution

The comparison of the calculated vertical excitation energies shows that ADC(2) (Fig. 6) performs better than TD-CAM-B3LYP (Fig. S4–S6) with respect to the experimental results. This is consistent with the benchmark of a large set of organic molecules where ADC(2) was shown to give 0.22 eV mean average error [65], while it was 0.30 eV for TD-CAM-B3LYP [81]. Therefore, in this section, we focus on the results obtained at ADC(2) level for methyl substituted retinal models.

In the comparison of different conformations of the single bonds connecting the polyene chain with the cyclohexenyl ring, the s-*cis* conformation was more stable than s-*trans*, as evidenced by the relative energetics listed in Table S1, for **10** and **11**. Therefore, the s-*cis* conformation was selected for the vertical excitation energies of **10** and **11**. For **12**, the s-*cis* and s-*trans* were within ~ 1 kcal·mol^{-1} of each other, and for the PSB models, the s-*trans* was more stable than the s-*cis*. Accordingly, the s-*trans* conformation was selected for the vertical excitation energies of **12**.

The calculated vertical excitation energies for the aldehyde models are compared with their experimental counterparts in Fig. 6a. The S_1 state had the highest oscillator strength among the three lowest excited states except for models $\mathbf{1}_{cis}$, $\mathbf{1}_{trans}$, **11,** and **12**, where the S_2 state had the highest oscillator strength. A similar result was reported

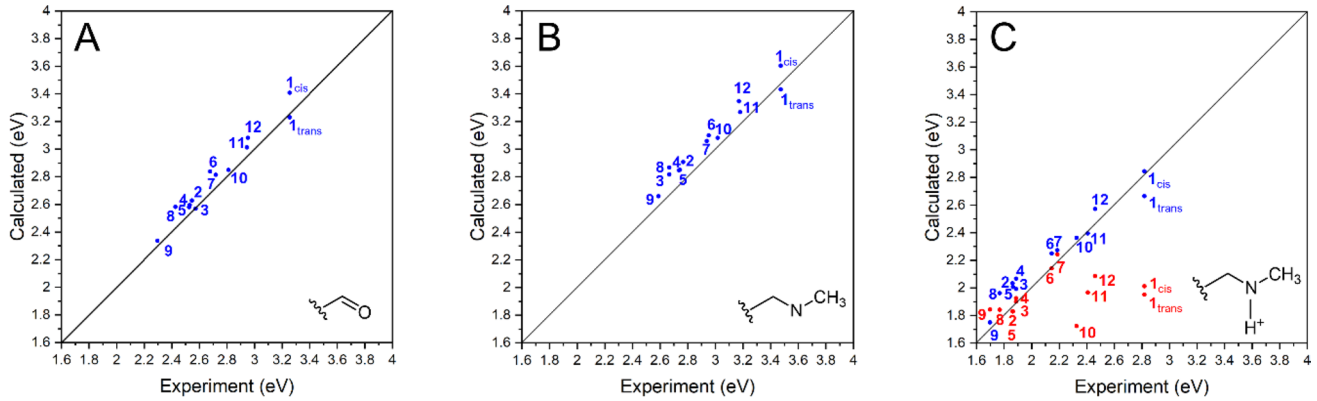

Fig. 6 Calculated excitation energies with ADC(2) in ethanol versus experimental λ^a_{max} values of PSB retinal models (**1**–**12**) including A) aldehyde, B) SB_{Me}, and C) PSB with and without the counterion (PSB_{Me} in red and PSB_{Me+Cl-} in blue, respectively)

for the multireference (extended multistate CASPT2) calculations for truncated retinal models in the gas phase [82]. However, the S_1 state became the bright state after adding solvent effects. The agreement between the calculated vertical excitation energies and the experimental absorption maxima (λ^a_{max}) improves upon inclusion of the implicit solvent model for ethanol. This is confirmed by the root-mean-square error (RMSE) change from 0.48 eV in the gas phase to 0.10 eV in solution (Figure S6).

In case of the SB_{Me} models, the inclusion of the solvent model also improves the calculated excitation energies (Fig. S7). The RMSE improves from 0.38 eV in the gas phase to 0.13 eV in ethanol solution. However, for the PSB_{Me} models, the RMSE is changing from 0.40 eV to 0.19 eV when going from gas phase to solvent model. It should be pointed out that the deviations between the computed and measured values for the models $\mathbf{1}_{cis}$, $\mathbf{1}_{trans}$, **10**, **11,** and **12** without a counterion are not negligible and range from 0.15 to 0.45 eV (Fig. 6C, red). It seems that the implicit solvent is failing to describe the excitation energies in these cases. This could be due to the implicit nature of the solvent, where a dielectric constant is applied on the surface of the molecule. This is in contrast to explicit solvent models which contain ethanol molecules. These five models with larger errors have one structural feature in common, namely a single bond which connects the polyene to their heterocycles. In all other models, except **10,** there is a double bond instead.

In addition to the PSB_{Me} models, we considered the effect of including a counterion ion and called these models PSB_{Me+Cl-}. To saturate the positive charge of the PSB, we added a chloride counterion in the proximity to the SB hydrogen (Fig. S3). Recent studies in the gas phase have already shown a strong blue shift of the excitation energy upon addition of a counterion [83]. Indeed, this has improved agreement with experiment for the 5 aforementioned models and lowered the total RMSE from 0.19 eV (PSB_{Me}) to 0.12 eV (PSB_{Me+Cl-}).

Table 2 Vertical excitations energies, their corresponding oscillator strengths, and opsin shifts of bR-**1** and bR-**2** from the ADC(2) calculations; (Δ)E = [bR-**1**] - []

	Experiment	ADC(2)		OS (cm^{-1})
	λ^a_{max} (eV)	λ^a_{max} (eV)	*f*	
bR-**1**	2.18	2.30	2.02	4436/2952*
bR-**2**	1.64	1.88	1.99	1264
ΔE**	0.54	0.42		

*, The values are computed for bR-**1** and the solvated PSB_{Me} $\mathbf{1}_{cis}$ and $\mathbf{1}_{trans}$*, respectively

, ΔE = [bR-1**] − [bR-**2**]

3.5 QM/MM simulations of bR

The excitation energies of bR-**1** and bR-**2** are reported in Table 2 for ADC(2) and Table S3 for TD-CAM-B3LYP. The deviation from the experimental λ^a_{max} for bR-**1** is smaller for ADC(2) (0.12 eV) than for TD-CAM-B3LYP (0.83 eV). A similar trend is observed for the chromophore bR-**2** where the ADC(2) excitation energy deviates by 0.24 eV, while for TD-CAM-B3LYP results in a large error of 1.14 eV. Nevertheless, both methods reproduce the red shift of bR-**2** relative to bR-**1**. The ΔE (the difference between the excitation energies of bR-**1** and bR-**2**) was 0.54, 0.42, and 0.22 eV for experiment, ADC(2), and TD-CAM-B3LYP, respectively. This is in line with the previous calculations of retinal in different opsin mutants [58]. Since ADC(2) performed better than TD-CAM-B3LYP for the excitation energy calculations, we will focus our OS discussion on the ADC(2) calculations.

The values are computed for bR-1and the solvated PSBMe 1cis and 1trans*, respectively. The results in the

protein can also be used to compute the OS, which is defined as the difference between the absorption of retinal PSB in the protein environment and in solution. For the retinal PSB, the experimental value is 5183 cm^{-1}. For ADC(2), the OS is 4436 and 2952 cm^{-1}, if the solvated reference is based on $\mathbf{1}_{cis}$ or $\mathbf{1}_{trans}$, respectively. In case of the derivative **2,** the experimental shift is 1770 cm^{-1}, while the computed value is 1264 cm^{-1}. The experimental trend of the opsin shift is qualitatively reproduced, namely the significant larger shift of retinal compared to compound **2** when changing the environment from solution to protein.

We also analyzed the protein–chromophore interactions of bR-**2** relative to bR-**1** by generating electrostatic potential maps (Fig. 7). In one case, we visualized the projection of the electrostatic potentials from the protein environment on the chromophores (top panels, Fig. 7). Here, the counterions Asp85 and Asp212 are the main source of negative charge imparted at the iminium nitrogen of both chromophores in bR-**1** and bR-**2**. The negative charge (indicated by the red shading in Fig. 7, top panels) is distributed similarly on **1** and **2**, as expected. In the other case, the protein charges are disregarded and the electrostatic potentials associated with the chromophores are visualized (Fig. 7, lower panels). Here, **1** and **2** carried overall positive charges, due to the PSB. For **2**, the positive charge is more delocalized across the chromophore in comparison to **1**, where the positive charge is localized around the iminium nitrogen. The shift of the positive charge towards the heterocycle in **2** could contribute to a smaller OS relative to bR-**1** (Table 2). This is also supported by the resonance structure VII (Scheme 2) which show the positive charge to be localized on the second nitrogen of **2**, instead of carbon in **1**. This leads to a stabilization of the resonance structure which is contributing to the excited-state electronic structure and therefore lowering the excitation energy.

Interestingly, the electrostatic picture of bR-**2** in the ground state resembles what is expected to occur in the excited state for retinal proteins, i.e., the positive charge shifts away from the PSB towards the cyclohexenyl ring. The shift of the positive charge towards the heterocycle in **2** could contribute to a smaller OS relative to bR-**1** (Table 2). This is mainly because the negative charge from the protein environment matches the positive charge of the chromophore itself in bR-**1** which is apparent from the visualization in Fig. 7. Although the OS is greater for **1** than **2**, bR-**2** is still more red-shifted than bR-**1** due to an intrinsic property of **2** which seems to be independent of the protein environment.

3.6 Retinal exchange experiments

Since the λ^{a}_{max} values of the PSBs capable of forming bRs (**2**–**6**, **8**, **9**) are strongly red-shifted compared to that of retinal, small OSs resulted for these compounds and retinal exchange experiments were performed to check whether a weak or non-covalent binding between the protein and the chromophores took place. Accordingly, the newly formed pigments were incubated with all-*trans* retinal allowing a simple adsorption to the membrane or unspecific attachment to the protein in the formation of bR. However, bR formation was not observed in any case. Incubation with merocyanine **10** yielded bR-**10** with a relatively blue-shifted, broad absorption band (λ^{a}_{max} = 533 nm, Fig. 5b) and no bR formation could be observed upon addition of retinal. In the opposite case, however, when compound **10** was added to a bR suspension, an additional absorption band around 540 nm, similar to those found from direct assembly, was

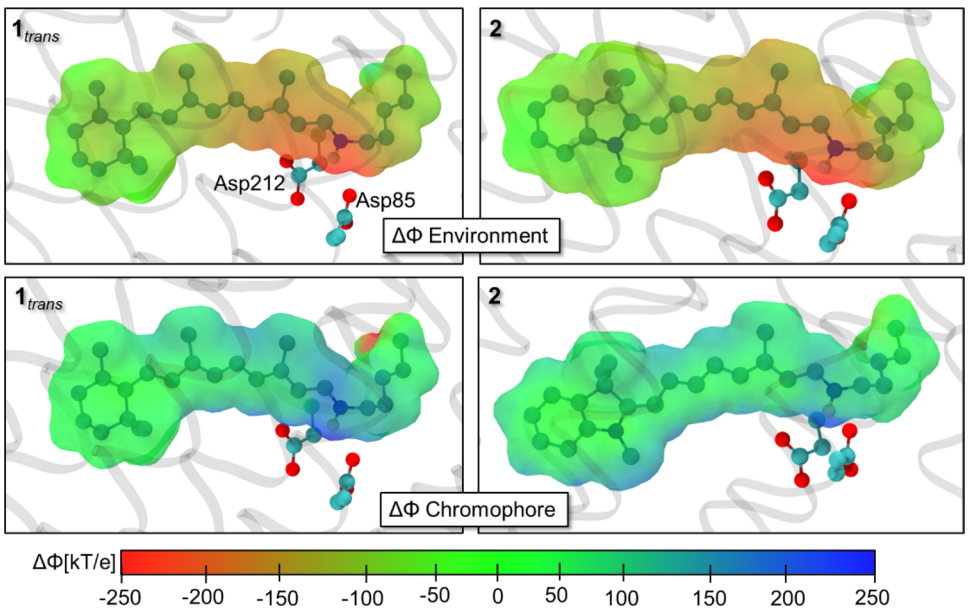

Fig. 7 The electrostatic potentials of bR-**1** and bR-**2** with the Asp counterions. The top panels show the charges of the protein on the chromophore, whereas the bottom panels show the charges of the chromophore alone. The APBS program was used to determine the electrostatic potentials and they were visualized in VMD [84, 85].

observed. This nearly identical absorption maximum indicates a specific interaction with bO, such that this compound only adsorbs to the protein, albeit in a way which apparently interferes with the binding of retinal.

The failure in reconstitution with compounds **7**, **10**–**12** demonstrates the steric constraints of the ring-binding site (compare **6** and **10**, **11**) of the protein, but also the demand of an exact fitting of the chromophore into the protein cavity around the polyene chain positions 13 and 14 ('retinal numbering', *cf*. **6** and **7**, **12**). It is worth noting that for merocyanines with four double bonds, a rearrangement of the substitution pattern in the polyene chain, placing methyl groups at positions 11, 12, or 14 (retinal numbering, compounds **3**, **4**, **5**), is tolerated to a large extent by the protein-binding cavity, except of compound **7**, where assembly is inhibited, probably due to the cumulative effects of the presence of a methyl group at position 14 and a reduced polyene chain length (compare bRs-**6** and -**7**).

This result is in contrast to retinal-type chromophores where a change of the methyl group substitution pattern is not accepted by the protein-binding site [35, 86]. Among compounds **2**–**5**, which solely differ by the position of the methyl groups in the polyene chain, only merocyanine **2** is practically undisturbed in the protein-binding site. The direct comparison of bR-**2** with bR-**3**, which carries a side chain with equal length and differs only by the position of the methyl group in the polyene chain (position 13 vs. 14), demonstrates the constraints from the binding pocket (Fig. 8). Both bR-derivatives show absorption bands practically identical in shape (including the shoulder at the high-energy side of the band) but are shifted by 55 nm with respect to the position of their λ^{a}_{max} (700 vs. 755 nm, bR-**3** vs. bR-**2**, respectively).

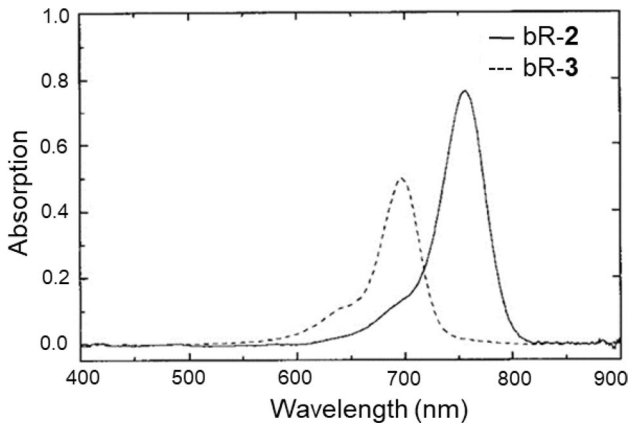

Fig. 8 Absorption spectra of bR-**2** and bR-**3**

3.7 pH-dependence of bRs

Titration of the reconstituted bRs to high pH values (pH 9) led to deprotonation of the SB which becomes obvious from—depending on the pK_a value of the investigated hemicyanine chromophore—a reduction or disappearance of the bathochromic absorption band and a concomitant formation of a blue-shifted, broad absorption band of low intensity. This is shown for bR-**2** (Fig. 9, top) and bR-**8** (Fig. 9, bottom, note that an increase of the pH value caused increased scattering in the absorption spectrum). Both bR-derivatives differ in their pK_a values, but for both samples, the pK_a value is clearly lower than that of native bR. Apparently, the pK_a value of bR-**2** is higher than that of bR-**8**, since the amplitude and position of its absorption band remains unchanged, starting from pH 4 and going via pH 6 to 7.5. Only upon adjustment of the pH to 9.0, a strong reduction of the absorption band is seen together with the appearance of a new, broad absorption around 620 nm, but still, an absorption around 755 nm remains. For bR-**8**, the increase from pH 4 to pH 6 causes a reduction in intensity of the absorption band around 740 nm, an effect which is more pronounced at pH 7.5. Adjustment of the pH to 9.0 in this pigment causes a complete conversion into the unprotonated SB with a broad absorption band around 630 nm.

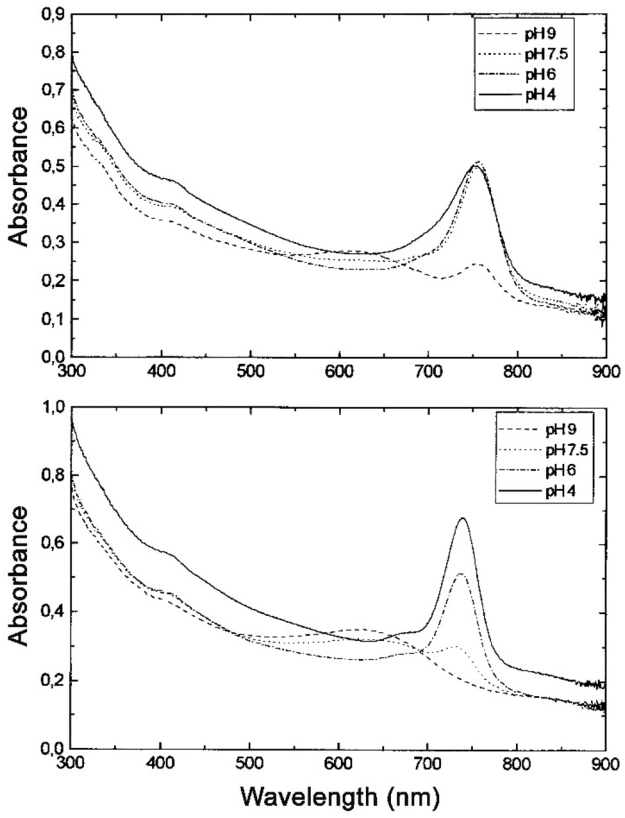

Fig. 9 pH dependences of bR-**2** (top) and bR-**8** (bottom)

Table 3 Fluorescence properties of the aldehydes of compounds **1**–**12** and their assembly products with bO

	Aldehyde			bR				
	λ^{a}_{max} (nm)	λ^{f}_{em} (nm)	$\Delta_{Stokes\text{-}shift}$ (cm^{-1})	λ^{a}_{max} (nm)	λ^{f}_{em} (nm)		Φ_f	$\Delta_{Stokes\text{-}Shift}$ (cm^{-1})
1	381		600	9649	570	740	1.5×10^{-5}	4030
2	487		678	5785	755	779	0.10	408
3	482		663	5664	700	719	0.15	378
4	490		660	5257	651[a]	695[a]	~0.18	1099
					698[a]	698[a]	~0.05	
5	491		675	5552	711[b]	735[b]	0.03	459
6	463		580	4357	610	635	N/A	645
7	456		561	4105	–[c]	–[c]	N/A	–[c]
8	511		696	5202	736	757	0.07	377
9	540		678	3769	766	791	0.02	413
10	441		705	8491	–[c]	–[c]	0.004	–
11	421		618	7572	–[c]	–[c]	0.01	–
12	420		570	6266	–[c]	–[c]	0.002	–

[a]There are two isomers present with partially overlapping absorption bands

[b]No complete reconstitution between 5 and bO

[c]No covalent chromophore protein binding (for details, see results section)

3.8 Fluorescence spectroscopy

As expected for merocyanine compounds, aldehydes **2**–**12** in organic solvents showed a much stronger fluorescence than retinal and exhibited relatively small Stokes shifts (retinal: 9649 cm^{-1}, Table 3). The smallest value of those compounds carrying four double bonds in the polyene chain was determined for **9** (3769 cm^{-1}), whereas the largest value was found for **10** (8491 cm^{-1}). Clearly, the chain length has an influence on the Stokes shift (*cf.* **6**, **7**), but also the electronic structure of the ring moiety and its connection to the polyene chain, as is evident from a comparison with the values of **11** and **12**. Although both compounds carry a side chain of only three double bonds, the shifts are already larger than those of the "full-length" compounds (7572 and 6266 cm^{-1}, respectively). For **11** and **12**, a single bond connects the ring end group with the polyene chain giving a higher flexibility of the retinal derivative and this might contribute to the large Stokes shifts.

When fluorescence spectra were recorded for the reconstituted bRs (carrying merocyanines **2**–**6**, **8**, **9**), the difference between the Stokes shifts for bR and the hemicyanine-bRs is even larger than for the free compounds in organic solvents. Whereas bR exhibits a Stokes shift of 4030 cm^{-1}, the corresponding values were in the order of 400 cm^{-1}, with the exception of **4** and **6**, for which shifts of 1099 and 645 cm^{-1}, respectively, were determined (Table 3). The absorption and fluorescence emission spectra of compound **2** in EtOH and the bR-**2** are shown in Fig. 10.

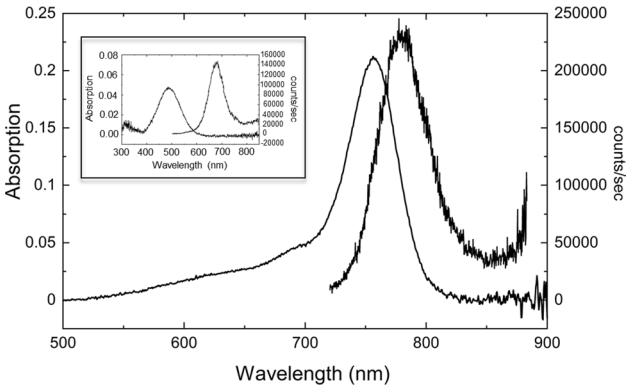

Fig. 10 Absorption and emission spectra of (insert) **2** (in EtOH) and of bR-**2**

Besides the smaller Stokes shift, the retinal analogues have an increased fluorescence quantum yield, Φf. The largest increase was noted for bR-**4** and -**3**, namely 0.18 and 0.15, which is of similar magnitude as the naturally occurring NeoR which has a Φf of 0.2 [59, 87]. This is one order of magnitude larger than Φf obtained by site-directed mutagenesis. For example, Hegemann and coworkers reported variants of Archon1 that reached almost Φf of 0.01 [88]. Its mechanism was recently reported in a computational study by Barneschi et al. [89]

3.9 Photochemical activity of reconstituted bR analogues

A literature survey revealed that out of the several merocyanine compounds that were incorporated into bO, only one case of photochemical activity has been reported [46]. These scholars incorporated 7-(1′-pyrrolidine)-2,4,6-heptatrienal into bO (λ_{max}: 530 nm) and subjected this pigment to flash photolysis. A bathochromic, short-lived intermediate was detected (λ_{max}: 570 nm) that directly reverted to the initial state.

As already described in a short communication, bRs formed from compounds **4** and **5** did not undergo a photocycle in a bR-like manner [35]. Also bRs containing the other pigment-forming compounds **2**, **3**, **6**, **8**, and **9** showed an entirely unknown photochemical reactivity. It has to be stated here that such light responses are without examples in the literature and, thus, any interpretation on the light-induced and following thermally driven molecular changes of these pigments is partly speculative and has to be performed with great care.

Laser flash experiments performed with all analogue bRs did not yield any identifiable absorption changes within the time resolution of the instrument (ca. 50 ns). Thus, further experiments were performed with continuous white light illumination for several minutes (5–10 min), or, in few cases, with interference filters aiming to selectively irradiate within the major absorption band. Three types of photochemical responses were observed: bRs carrying merocyanines **2**, **3**, and **6** did not show any absorption changes after white light illumination for 10 min. We note here that, if illumination of bR-**2** is performed with an incompletely assembled protein, but in the presence of an excess of free chromophore, the absorption band increased strongly after switching off the light source, indicative that white light causes isomerization of the free chromophore yielding an isomeric form that can enter the chromophore pocket and bind to the protein. bR-**2** shows a further unexpected behavior if illumination is performed with narrow band interference filter (see below). Upon white light illumination, a reduction in absorption band intensity resulted for bRs containing **8** and **9**, by 40% (**8**) and 20% (**9**). Interestingly, if retinal was added to the pigments after illumination, native bR was formed (λ_{max}: 568 nm). This result points to a hydrolysis of the bO-hemicyanine PSB and a preferred binding of retinal to the open binding site. The observable reduction of the absorption bands of these two pigments (**8** and **9**) without any shift of the absorption maximum and the ready assembly of the bO-binding site and retinal points to a photochemically induced destruction of the two chromophores after or concurrent with a hydrolysis of the PSB. With all careful speculation, one may state that these chromophores are bound in a distorted conformation with a certain probability of triplet formation in the excited state at one of the strongly twisted double bonds that then can become target of triplet oxygen attack. Photochemical activity with observable intermediates was found only for bRs-**4** and -**5**, as was already outlined in the short communication [35]. For both pigments, white light illumination (10 min) caused an only small reduction of the absorption band (around 2%) that is followed by a very slow thermally driven process of further intensity reduction of the absorption band concomitant with the growth of a hypsochromically shifted new absorption band (referring to bR-**4**, λ_{max}: 698 nm, intermediate-**4**, λ_{max}: 654 nm). Further incubation in the dark shows a reversion of the intermediate-forming process back to the initial state. During both the thermal forward and the backward reactions, the absorption bands show the same isosbestic point at ca. 660 nm. These changes in absorbance might be interpreted as a photoisomerization at one double bond resulting in a strongly contorted conformation, yet with the same absorption maximum as the dark state. As, apparently, a direct thermal reformation of the dark state is impossible, the chromophore undergoes in the dark further conformational changes during which the short-wavelength intermediate is formed. It may be speculated that a further double bond is isomerized, then allowing the chromophore to re-convert into the initial dark state. We may state here that we could not follow these conformational changes by any analytical or spectroscopic method. The photochemical activity under white light of bRs-**4** and -**5**, and the above described generation of an isomer of chromophore **2** in solution capable to increase the absorption of bR-(λ_{max}: 568 nm) point to a photoisomerization and asked for more defined illumination conditions. Irradiation with an interference filter ($\lambda_{exc} = 731 \pm 10$ nm) for 10 min yielded for bRs-**4** and -**5** very similar absorption changes as observed for white light illumination. Whereas

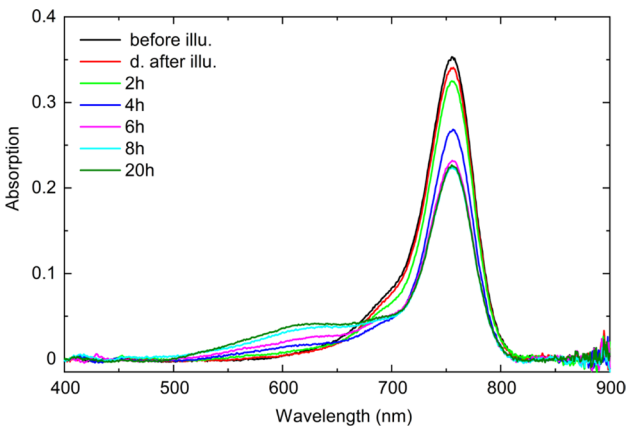

Fig. 11 Light induced reactions of merocyanine bR-**2**

illumination of the pigment carrying compound **2** with white light did not change the absorption band (see above), the use of the narrow band filter revealed a photochemical reaction similar as those of bRs-**4** and -**5**. Directly after finishing the 10 min illumination, a small decrease in the intensity of the absorption band was recorded (reduction by ca. 5%). Following an incubation in the dark showed, as for bRs-**4** and -**5**, a very slow change of the absorption band. During a time course of 20 h, the maximum band at 755 nm lost intensity and a new, very broad absorption band around 620 nm were formed (Fig. 11), which remained stable over long periods of time. In contrast to the bR-**4**, the parent state of bR-**2** was not reformed. Notably, those merocyanines that showed photochemical activity under white light (bRs-**4** and -**5**) carry their side chain methyl groups at 'wrong' positions (position 12 or 11 in retinal numbering), whereas bR-**2** with a methyl group at position 13 only under inference filter conditions undergoes a photochemical reaction.

The absence of a photocycle akin to that of bR had already been observed in preliminary experiments, which also revealed a different type of photochemistry for this class of compounds [14]. The fluorescence quantum yields (Φf) collected in Table 3 underscore the distinct photochemical behavior of the analogue bRs compared to native bR. In bR, the Φf is $1.5 \cdot 10^{-5}$, whereas the analogue bRs exhibit Φf's up to several orders of magnitude greater than bR. For example, the Φf of the N-methyl-3,3-dimethylindolylidene containing merocyanines, bR-**4**, bR-**3**, and bR-**2**, was significantly greater than bR at 0.18, 0.15, and 0.10, respectively. For the bR analogues, there seems to be a stronger influence of fluorescence in the competition with photoisomerization than in bR. A detailed analysis for all these merocyanine compounds in this work demonstrates two counteracting forces, namely, the attempt to maintain the fully conjugated character of these compounds, on the one hand, and the influence of the protein-binding site required for photoisomerization at a selected double bond, on the other hand. In consequence of this situation, for some of the merocyanines, the covalent bond to the protein is disrupted upon illumination (see formation of bR upon addition of retinal to the irradiated bR analogues carrying compounds **8** and **9**), and, without addition of retinal, it can be reformed during long time periods [35, 80]. It is worth noting that the initial conformational changes of the excited chromophore are probably transduced to the protein environment, inducing structural changes that repel the chromophore from the binding pocket. This result might add to the discussion as to whether a non-isomerizable chromophore can induce structural changes in the protein [18]. Overall, the merocyanine compounds may in general adopt a slightly different position or conformation in the protein cavity that upon illumination allows a facilitated hydrolysis of the SB. One could assume that the chromophore photoisomerizes, probably at a different position than retinal, which causes a strong steric hindrance and facilitates hydrolysis of the SB. Such a proposal concurs with the observed lower pK_a values of the bR-derivatives.

The photochemical activity, outlined here for compounds **2**, **4**, and **5**, is apparently very inefficient, requiring long irradiation periods, and is entirely different from that of native bR. Such slow processes impede quantitative time-resolved measurements. As an observable result, a blue-shifted absorption band appears as a thermally driven process over long periods of time (many minutes or even hours), which then, in some cases and in an even slower reaction, reforms the bathochromic hemicyanine-typical absorption. As no further structural information is available, an interpretation of the light-driven reactions remains speculative, as was posted already at the beginning of the photochemical description. The blue-shifted intermediates, seen for several of these hemicyanine-bOs, apparently originate from a light-induced, modified structure or conformation of the chromophore, which cannot reform the parent state directly (probably also due to changes of the protein environment), but allows only the formation of the hypsochromic intermediate. Even from this somehow distorted intermediate, the formation of the original bathochromically absorbing form has to overcome a large activation energy barrier, as is seen from the hours-lasting recovery kinetics.

4 Conclusion

The synthesis of a series of merocyanines with hetero-aromatic ring end groups and their incorporation with bO adds novel insights into the chromophore–protein interactions in bR. The absorption maxima of the free aldehydes, SBs, and PSBs of compounds **2**–**12** exhibit absorption maxima which are bathochromically shifted compared to their respective forms in retinal. Quantum chemical calculations, performed in parallel, successfully concurred with the experimental trends in absorption maxima.

Notably, already the PSBs of these merocyanines in ethanol are red-shifted relative to retinal in bR (λ^a_{max} = 570 nm) except **7** and **10**–**12**; these latter compounds did not assemble in a clear form with bO (note the discussion of **10** in the main text). The successfully assembled bRs showed strongly red-shifted absorption maxima, some of which reaching out into the near-IR range, yet with smaller values for their OS. This leads to the conclusion that the merocyanine structure itself is not fully responsible for the observed red shifts in the bRs, but and rather, there is some contribution from the protein, however, of lower intensity than in bR. This is well documented upon inspection of Fig. 7 which compares the electrostatic potentials of bR-**1** and bR-**2** from QM/MM calculations. In comparison to

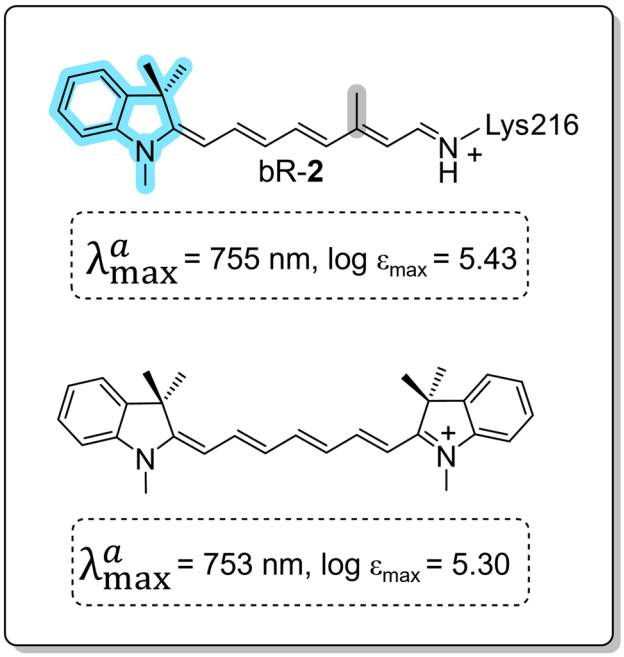

Scheme 3 Effect of a symmetrical electronic structure on the λ^{a}_{max} and ε_{max} values in a symmetrical cyanine compound [71]

bR-**1**, the positive charge of the chromophore of bR-**2** is delocalized. The strongly bathochromic and narrow absorption bands, small Stokes' shifts, and also the much larger fluorescence of the analogue bRs (compared to that of retinal or bR) identify their merocyanine and hemicyanine character (upon formation of SBs). The photochemical reactions were found to be entirely different from that of bR due to altered (more conjugated) electronic structures of these compounds resulting in a complete loss or an unprecedented response to irradiation, still calling for a characterization of the processes on a molecular level. Considering the unexpected photochemical activity, it appears unlikely that a proton pumping activity would be recorded; however, this remains to be tested in future experiments.

The interesting potential of these compounds lies in their extremely bathochromic absorption and their even further red-shifted fluorescence. This feature was already demonstrated in living cells when molecule **2** was used in Arch to shift the fluorescence to the NIR [48]. Following this, future applications in imaging and optogenetics can be imagined (Scheme 3).

Supplementary Information The online version contains supplementary material available at https://doi.org/10.1007/s43630-023-00496-0.

Acknowledgements The authors thank Dr. Marvin Asido (Goethe-Universität Frankfurt am Main) for providing the bR UV/Vis absorption spectrum. Megan J. Mackintosh thanks the Zuckerman STEM Leadership Program for their support. Igor Schapiro acknowledges the German Research Foundation via the SFB 1078 project C6, and he is also thankful for the support by the Israel Science Foundation (Research Center Grant No. 3131/20) and the GIF NEXUS No. I-1560-207.9/2023.

Funding Open Access funding enabled and organized by Projekt DEAL.

Data availability The data of this study are available from the corresponding authors upon reasonable request.

Declarations

Conflict of interest On behalf of all authors, the corresponding author (WG) states that there is no conflict of interest.

References

1. Lanyi, J. K. (1997). Mechanism of ion transport across membranes: Bacteriorhodopsin as a prototype for proton pumps. *Journal of Biological Chemistry, 272*(50), 31209–31212.
2. Haupts, U., Tittor, J., & Oesterhelt, D. (1999). Closing in on bacteriorhodopsin: Progress in understanding the molecule. *Annual Review of Biophysics and Biomolecular Structure, 28*(1), 367–399.
3. Landau, E. M., Pebay-Peyroula, E., & Neutze, R. (2003). Structural and mechanistic insight from high resolution structures of archaeal rhodopsins. *FEBS Letters, 555*(1), 51–56.
4. Oesterhelt, D. (1998). The structure and mechanism of the family of retinal proteins from halophilic archaea. *Current Opinion in Structural Biology, 8*(4), 489–500.
5. Nakanishi, K., Balogh-Nair, V., Arnaboldi, M., Tsujimoto, K., & Honig, B. (1980). An external point-charge model for bacteriorhodopsin to account for its purple color. *Journal of the American Chemical Society, 102*(27), 7945–7947.
6. Schulten, K., Dinur, U., & Honig, B. (2008). The spectra of carbonium ions, cyanine dyes, and protonated Schiff base polyenes. *The Journal of Chemical Physics, 73*(8), 3927–3935.
7. Honig, B., Greenberg, A. D., Dinur, U., & Ebrey, T. G. (1976). Visual-pigment spectra: Implications of the protonation of the retinal Schiff base. *Biochemistry, 15*(21), 4593–4599.
8. Kropf, A., & Hubbard, R. (1958). The mechanism of bleaching rhodopsin. *Annals of the New York Academy of Sciences, 74*(2), 266–280.
9. Balogh-Nair, V., Carriker, J. D., Honig, B., Kamat, V., Motto, M. G., Nakanishi, K., Sen, R., Sheves, M., Tanis, M. A., & Tsujimoto, K. (1981). The 'Opsin Shift' in bacteriorhodopsin: Studies with artificial bacteriorhodopsins. *Photochemistry and Photobiology, 33*(4), 483–488.

10. Honig, B., Dinur, U., Nakanishi, K., Balogh-Nair, V., Gawinowicz, M. A., Arnaboldi, M., & Motto, M. G. (1979). An external point-charge model for wavelength regulation in visual pigments. *Journal of the American Chemical Society, 101*(23), 7084–7086.
11. Nakanishi, K., Balogh-Nair, V., Gawinowicz, M. A., Arnaboldi, M., Motto, M., & Honig, B. (1979). Double point charge model for visual pigments; Evidence from dihydrorhodopsins. *Photochemistry and Photobiology, 29*(4), 657–660.
12. Kakitani, H., Kakitani, T., Rodman, H., & Honig, B. (1985). On the mechanism of wavelength regulation in visual pigments. *Photochemistry and Photobiology, 41*(4), 471–479.
13. Rajamani, R., & Gao, J. (2002). Combined QM/MM study of the opsin shift in bacteriorhodopsin. *Journal of Computational Chemistry, 23*(1), 96–105.
14. Rajamani, R., Lin, Y.-L., & Gao, J. (2011). The opsin shift and mechanism of spectral tuning in rhodopsin. *Journal of Computational Chemistry, 32*(5), 854–865.
15. Irving, C. S., Byers, G. W., & Leermakers, P. A. (1970). Spectroscopic model for the visual pigments. *Influence of microenvironmental polarizability. Biochemistry, 9*(4), 858–864.
16. Yan, B., Spudich, J. L., Mazur, P., Vunnam, S., Derguini, F., & Nakanishi, K. (1995). Spectral tuning in bacteriorhodopsin in the absence of counterion and coplanarization effects. *Journal of Biological Chemistry, 270*(50), 29668–29670.
17. Houjou, H., Inoue, Y., & Sakurai, M. (1998). Physical origin of the opsin shift of bacteriorhodopsin. Comprehensive analysis based on medium effect theory of absorption spectra. *Journal of the American Chemical Society, 120*(18), 4459–4470.
18. Mathies, R. A., Lin, S. W., Ames, J. B., & Pollard, W. T. (1991). From femtoseconds to biology: Mechanism of bacteriorhodopsin's light-driven proton pump. *Annual Review of Biophysics and Biophysical Chemistry, 20*(1), 491–518.
19. Van der Steen, R., Biesheuvel, P. L., Mathies, R. A., & Lugtenburg, J. (1986). Retinal analogs with locked 6–7 conformations show that bacteriorhodopsin requires the 6-s-trans conformation of the chromophore. *Journal of the American Chemical Society, 108*(20), 6410–6411.
20. Harbison, G. S., Smith, S. O., Pardoen, J. A., Courtin, J. M. L., Lugtenburg, J., Herzfeld, J., Mathies, R. A., & Griffin, R. G. (1985). Solid-state carbon-13 NMR detection of a perturbed 6-s-trans chromophore in bacteriorhodopsin. *Biochemistry, 24*(24), 6955–6962.
21. Wada, M., Sakurai, M., Inoue, Y., Tamura, Y., & Watanabe, Y. (1994). Ab initio study of 13C NMR chemical shifts for the chromophores of rhodopsin and bacteriorhodopsin. 1. Theoretical estimation of their ring-chain conformations. *Journal of the American Chemical Society, 116*(4), 1537–1545.
22. Borshchevskiy, V., Kovalev, K., Round, E., Efremov, R., Astashkin, R., Bourenkov, G., Bratanov, D., Balandin, T., Chizhov, I., Baeken, C., Gushchin, I., Kuzmin, A., Alekseev, A., Rogachev, A., Willbold, D., Engelhard, M., Bamberg, E., Büldt, G., & Gordeliy, V. (2022). True-atomic-resolution insights into the structure and functional role of linear chains and low-barrier hydrogen bonds in proteins. *Nature Structural & Molecular Biology, 29*(5), 440–450.
23. Wickstrand, C., Dods, R., Royant, A., & Neutze, R. (2015). Bacteriorhodopsin: Would the real structural intermediates please stand up? *Biochimica et Biophysica Acta (BBA) - General Subjects, 1850*(3), 536–553.
24. Nakanishi, K., & Crouch, R. (1995). Application of artificial pigments to structure determination and study of photoinduced transformations of retinal proteins. *Israel Journal of Chemistry, 35*(3–4), 253–272.
25. van der Steen, R., Biesheuvel, P. L., Lugtenburg, J., Erkelens, C., & Mathies, R. A. (1989). 8,16- and 8,18-methanobacteriorhodopsin. Synthesis and spectroscopy of 8,16- and 8,18-methanoretinal and their interaction with bacterioopsin. *Recueil des Travaux Chimiques des Pays-Bas, 108*(3), 83–93.
26. Albeck, A., Livnah, N., Gottlieb, H., & Sheves, M. (1992). Carbon-13 NMR studies of model compounds for bacteriorhodopsin: Factors affecting the retinal chromophore chemical shifts and absorption maximum. *Journal of the American Chemical Society, 114*(7), 2400–2411.
27. Singh, A. K., Das, J., & Majumdar, N. (1996). Novel bacteriorhodopsin analogues based on azo chromophores. *Journal of the American Chemical Society, 118*(26), 6185–6191.
28. de Grip, W. J., & Ganapathy, S. (2022). Rhodopsins: An excitingly versatile protein species for research, development and creative engineering. *Frontiers in Chemistry, 10*, 879609.
29. Crouch, R. K. (1986). Studies of rhodopsin and bacteriorhodopsin using modified retinals. *Photochemistry and Photobiology, 44*(6), 803–807.
30. Ottolenghi, M., & Sheves, M. (1989). Synthetic retinals as probes for the binding site and photoreactions in rhodopsins. *The Journal of Membrane Biology, 112*(3), 193–212.
31. de Grip, W. J., van Oostrum, J., Bovee-Geurts, P. H. M., van der Steen, R., van Amsterdam, L. J. P., Groesbeek, M., & Lugtenburg, J. (1990). 10,20-Methanorhodopsins: (7E, 9E, 13E)-10, 20-methanorhodopsin and (7E, 9Z, 13Z)-10, 20-methanorhodopsin. *European Journal of Biochemistry, 191*(1), 211–220.
32. Liu, R. S. H., Krogh, E., Li, X.-Y., Mead, D., Colmenares, L. U., Thiel, J. R., Ellis, J., Wong, D., & Asato, A. E. (1993). Analyzing the red-shift characteristics of azulenic, naphthyl, other ring-fused and retinyl pigment analogs of bacteriorhodopsin. *Photochemistry and Photobiology, 58*(5), 701–705.
33. Tierno, M. E., Mead, D., Asato, A. E., Liu, R. S. H., Sekiya, N., Yoshihara, K., Chang, C. W., Nakanishi, K., Govindjee, R., & Ebrey, T. G. (1990). 14-Fluorobacteriorhodopsin and other fluorinated and 14-substituted analogs. An extra, unusually red-shifted pigment formed during dark adaptation. *Biochemistry, 29*(25), 5948–5953.
34. Motto, M. G., Sheves, M., Tsujimoto, K., Balogh-Nair, V., & Nakanishi, K. (1980). Opsin shifts in bovine rhodopsin and bacteriorhodopsin. Comparison of two external point-charge models. *Journal of the American Chemical Society, 102*(27), 7947–7949.
35. Hoischen, D., Steinmüller, S., Gärtner, W., Buss, V., & Martin, H.-D. (1997). Merocyanines as extremely bathochromically absorbing chromophores in the halobacterial membrane protein bacteriorhodopsin. *Angewandte Chemie International Edition in English, 36*(15), 1630–1633.
36. Sheves, M., Friedman, N., Albeck, A., & Ottolenghi, M. (1985). Primary photochemical event in bacteriorhodopsin: Study with artificial pigments. *Biochemistry, 24*(5), 1260–1265.
37. Tavan, P., Schulten, K., & Oesterhelt, D. (1985). The effect of protonation and electrical interactions on the stereochemistry of retinal Schiff bases. *Biophysical Journal, 47*(3), 415–430.
38. Asato, A. E., Mead, D., Denny, M., Bopp, T. T., & Liu, R. S. H. (1982). New geometric isomers of vitamin A and carotenoids. XI. 19,19,19-trifluororetinal and 20,20,20-trifluororetinal. *Journal of the American Chemical Society, 104*(18), 4979–4981.
39. Derguini, F., Caldwell, C. G., Motto, M. G., Balogh-Nair, V., & Nakanishi, K. (1983). Bacteriorhodopsins containing cyanine dye chromophores. Support for the external point-charge model. *Journal of the American Chemical Society, 105*(3), 646–648.
40. Kakitani, T., Kakitani, H., Honig, B., & Nakanishi, K. (1983). Symmetric charge distribution in the bacteriorhodopsin binding site. *Journal of the American Chemical Society, 105*(3), 648–650.
41. Ganapathy, S., Kratz, S., Chen, Q., Hellingwerf, K. J., de Groot, H. J. M., Rothschild, K. J., & de Grip, W. J. (2019). Redshifted and near-infrared active analog pigments based upon archaerhodopsin-3. *Photochemistry and Photobiology, 95*(4), 959–968.

42. Ganapathy, S., Venselaar, H., Chen, Q., de Groot, H. J. M., Hellingwerf, K. J., & de Grip, W. J. (2017). Retinal-based proton pumping in the near infrared. *Journal of the American Chemical Society, 139*(6), 2338–2344.
43. Hontani, Y., Ganapathy, S., Frehan, S., Kloz, M., de Grip, W. J., & Kennis, J. T. M. (2018). Strong pH-dependent near-infrared fluorescence in a microbial rhodopsin reconstituted with a red-shifting retinal analogue. *The Journal of Physical Chemistry Letters, 9*(22), 6469–6474.
44. Mei, G., Mamaeva, N., Ganapathy, S., Wang, P., DeGrip, W. J., & Rothschild, K. J. (2020). Analog retinal redshifts visible absorption of QuasAr transmembrane voltage sensors into near-infrared. *Photochemistry and Photobiology, 96*(1), 55–66.
45. Asato, A. E., Li, X. Y., Mead, D., Patterson, G. M. L., & Liu, R. S. H. (1990). Azulenic retinoids and the corresponding bacteriorhodopsin analogs. Unusually red-shifted pigments. *Journal of the American Chemical Society, 112*(20), 7398–7399.
46. Friedman, N., Sheves, M., & Ottolenghi, M. (1989). Model systems for rhodopsins: The photolysis of protonated retinal Schiff bases, cyanine dye, and artificial cyanine-bacteriorhodopsin. *Journal of the American Chemical Society, 111*(9), 3203–3211.
47. Shindy, H. A. (2017). Fundamentals in the chemistry of cyanine dyes: A review. *Dyes and Pigments, 145*, 505–513.
48. Herwig, L., Rice, A. J., Bedbrook, C. N., Zhang, R. K., Lignell, A., Cahn, J. K. B., Renata, H., Dodani, S. C., Cho, I., Cai, L., Gradinaru, V., & Arnold, F. H. (2017). Directed evolution of a bright near-infrared fluorescent rhodopsin using a synthetic chromophore. *Cell Chemical Biology, 24*(3), 415–425.
49. Becke, A. D. (1993). Density-functional thermochemistry. III. The role of exact exchange. *The Journal of Chemical Physics, 98*(7), 5648–5652.
50. Lee, C., Yang, W., & Parr, R. G. (1988). Development of the Colle–Salvetti correlation-energy formula into a functional of the electron density. *Physical Review B, 37*(2), 785–789.
51. Dunning, T. H., Jr. (1989). Gaussian basis sets for use in correlated molecular calculations. I. The atoms boron through neon and hydrogen. *The Journal of Chemical Physics, 90*(2), 1007–1023.
52. Grimme, S., Antony, J., Ehrlich, S., & Krieg, H. (2010). A consistent and accurate ab initio parametrization of density functional dispersion correction (DFT-D) for the 94 elements H-Pu. *The Journal of Chemical Physics, 132*(15), 154104.
53. Frisch, M. J., Trucks, G. W., Schlegel, H. B., Scuseria, G. E., Robb, M. A., Cheeseman, J. R., Scalmani, G., Barone, V., Petersson, G. A., Nakatsuji, H., Li, X., Caricato, M., Marenich, A., Bloino, J., Janesko, B. G., Gomperts, R., Mennucci, B., Hratchian, H. P., Ortiz, J. V., … Fox, D. J. (2009). *Gaussian 09, Revision B*. Gaussian, Inc.
54. Case, D. A., Betz, R. M., Cerutti, D. S., Cheatham, T. E., III., Darden, T. A., Duke, R. E., Giese, T. J., Gohlke, H., Goetz, A. W., Homeyer, N., Izadi, S., Janowski, P., Kaus, J., Kovalenko, A., Lee, T. S., LeGrand, S., Li, P., Lin, C., Luchko, T., … Kollman, P. A. (2016). *AMBER 2016*. University of California.
55. Case, D. A., Betz, R. M., Botello-Smith, W., Cerutti, D. S., Cheatham, T. E., III., Darden, T., Duke, R., et al. (2016). *AmberTools 16*. University of California.
56. Elstner, M., Porezag, D., Jungnickel, G., Elsner, J., Haugk, M., Frauenheim, T., Suhai, S., & Seifert, G. (1998). Self-consistent-charge density-functional tight-binding method for simulations of complex materials properties. *Physical Review B, 58*(11), 7260–7268.
57. Church, J. R., & Olsen, J. M., & Schapiro, I. (2022). The impact of retinal configuration on the protein–chromophore interactions in bistable jumping spider rhodopsin-1. *Molecules*, *27*(1), 71.
58. Church, J. R., Amoyal, G. S., Borin, V. A., Adam, S., Olsen, J. M. H., & Schapiro, I. (2022). Deciphering the spectral tuning mechanism in proteorhodopsin: The dominant role of electrostatics instead of chromophore geometry. *Chemistry – A European Journal, 28*(28), e202200139.
59. Broser, M., Spreen, A., Konold, P. E., Peter, E., Adam, S., Borin, V., Schapiro, I., Seifert, R., Kennis, J. T. M., Bernal Sierra, Y. A., & Hegemann, P. (2020). NeoR, a near-infrared absorbing rhodopsin. *Nature Communications, 11*(1), 5682.
60. Grimme, S., Ehrlich, S., & Goerigk, L. (2011). Effect of the damping function in dispersion corrected density functional theory. *Journal of Computational Chemistry, 32*(7), 1456–1465.
61. Liu, D. C., & Nocedal, J. (1989). On the limited memory BFGS method for large scale optimization. *Mathematical Programming, 45*(1), 503–528.
62. Tian, C., Kasavajhala, K., Belfon, K. A. A., Raguette, L., Huang, H., Migues, A. N., Bickel, J., Wang, Y., Pincay, J., Wu, Q., & Simmerling, C. (2020). ff19SB: Amino-acid-specific protein backbone parameters trained against quantum mechanics energy surfaces in solution. *Journal of Chemical Theory and Computation, 16*(1), 528–552.
63. Yanai, T., Tew, D. P., & Handy, N. C. (2004). A new hybrid exchange–correlation functional using the Coulomb-attenuating method (CAM-B3LYP). *Chemical Physics Letters, 393*(1), 51–57.
64. Schirmer, J. (1982). Beyond the random-phase approximation: A new approximation scheme for the polarization propagator. *Physical Review A, 26*(5), 2395–2416.
65. Dreuw, A., & Wormit, M. (2015). The algebraic diagrammatic construction scheme for the polarization propagator for the calculation of excited states. *WIREs Computational Molecular Science, 5*(1), 82–95.
66. Schäfer, A., Klamt, A., Sattel, D., Lohrenz, J. C. W., & Eckert, F. (2000). COSMO implementation in TURBOMOLE: Extension of an efficient quantum chemical code towards liquid systems. *Physical Chemistry Chemical Physics, 2*(10), 2187–2193.
67. Klamt, A., & Schuurmann, G. (1993). COSMO: A new approach to dielectric screening in solvents with explicit expressions for the screening energy and its gradient. *Journal of the Chemical Society, Perkin Transactions 2, 2*(5), 799–805.
68. TURBOMOLE V7.3 2018, a development of University of Karlsruhe and Forschungszentrum Karlsruhe GmbH, 1989-2007, TURBOMOLE GmbH, since 2007; available from http://www.turbomole.com.
69. Furche, F., Ahlrichs, R., Hättig, C., Klopper, W., Sierka, M., & Weigend, F. (2014). *WIREs Computational Molecular Science 4*(2), 91–100.
70. Hamanaka, T., Mitsui, T., Ashida, T., & Kakudo, M. (1972). The crystal structure of all-trans retinal1. *Acta Crystallographica Section B, 28*(1), 214–222.
71. Levitz, A., Marmarchi, F., & Henary, M. (2018). Synthesis and optical properties of near-infrared meso-phenyl-substituted symmetric heptamethine cyanine dyes *Molecules*, *23*(2), 226.
72. Mustroph, H. A.-O., & Towns, A. A.-O. (2018). Fine structure in electronic spectra of cyanine dyes: Are sub-bands largely determined by a dominant vibration or a collection of singly excited vibrations? *ChemPhysChem*, *19*(9), 1016–1023.
73. Mustroph, H., Reiner, K., Mistol, J., Ernst, S., Keil, D., & Hennig, L. (2009). Relationship between the molecular structure of cyanine dyes and the vibrational fine structure of their electronic absorption spectra. *ChemPhysChem, 10*(5), 835–840.
74. Pouradier, J. (1964). Remarque sur le spectre d'absorption des cyanines en solution. *J. Chim. Phys., 61*, 1107–1114.
75. West, W., & Geddes, A. L. (1964). The effects of solvents and of solid substrates on the visible molecular absorption spectrum of cyanine dyes. *The Journal of Physical Chemistry, 68*(4), 837–847.
76. West, W., & Pearce, S. (1965). The dimeric state of cyanine dyes. *The Journal of Physical Chemistry, 69*(6), 1894–1903.

77. Scheibe, G. (1966). Ergebnisse der Absorptionsspektroskopie hinsichtlich Lage, Intensität und Struktur der Banden. In W. Jung (Ed.), *Optische Anregung organischer Systeme* (pp. 109–159). Verlag Chemie.
78. Scheibe, G., Daltrozzo, E., Wörz, O., & Heiss, J. (1969). Das Franck–Condon–Prinzip und die Lichtabsorption von Merocyaninen. *Zeitschrift für Physikalische Chemie, 64*(14), 97–114.
79. Mustroph, H., Reiner, K., & Senns, B. (2017). Bond length alternation in unsymmetrical cyanine dyes and its influence on the vibrational structure of their electronic absorption spectra. *Coloration Technology, 133*(6), 469–475.
80. Hoischen, D. (1996). Synthese von heterocyclischen Retinoiden und Untersuchung ihrer Eigenschaften als prosthetische Gruppe in Bacteriorhodopsin der Weg zu Bathochrom absorbierenden, photoaktiven BR-Pigmenten. Dissertation, University of Düsseldorf, Germany.
81. Jacquemin, D., Wathelet, V., Perpète, E. A., & Adamo, C. (2009). Extensive TD-DFT benchmark: Singlet-excited states of organic molecules. *Journal of Chemical Theory and Computation, 5*(9), 2420–2435.
82. Filiba, O., Borin, V. A., & Schapiro, I. (2022). The involvement of triplet states in the isomerization of retinaloids. *Physical Chemistry Chemical Physics, 24*(42), 26223–26231.
83. Toker, Y., Langeland, J., Gruber, E., Kjær, C., Nielsen, S. B., Andersen, L. H., Borin, V. A., & Schapiro, I. (2018). Counterion-controlled spectral tuning of the protonated Schiff-base retinal. *Physical Review A, 98*(4), 043428.
84. Jurrus, E., Engel, D., Star, K., Monson, K., Brandi, J., Felberg, L. E., Brookes, D. H., Wilson, L., Chen, J., Liles, K., Chun, M., Li, P., Gohara, D. W., Dolinsky, T., Konecny, R., Koes, D. R., Nielsen, J. E., Head-Gordon, T., Geng, W., … Baker, N. A. (2018). Improvements to the APBS biomolecular solvation software suite. *Protein Science, 27*(1), 112–128.
85. Humphrey, W., Dalke, A., & Schulten, K. (1996). VMD: Visual molecular dynamics. *Journal of Molecular Graphics, 14*(1), 33–38.
86. de Lera, A. R., Iglesias, B., Rodriguez, J., Alvarez, R., Lopez, S., Villanueva, X., & Padros, E. (1995). Experimental and theoretical analysis of the steric tolerance of the binding site of bacterioopsin with the use of side-chain methyl-shifted retinal analogs. *Journal of the American Chemical Society, 117*(31), 8220–8231.
87. Palombo, R., Barneschi, L., Pedraza-González, L., Padula, D., Schapiro, I., & Olivucci, M. (2022). Retinal chromophore charge delocalization and confinement explain the extreme photophysics of neorhodopsin. *Nature Communications, 13*(1), 6652.
88. Silapetere, A., Hwang, S., Hontani, Y., Fernandez Lahore, R. G., Balke, J., Escobar, F. V., Tros, M., Konold, P. E., Matis, R., Croce, R., Walla, P. J., Hildebrandt, P., Alexiev, U., Kennis, J. T. M., Sun, H., Utesch, T., & Hegemann, P. (2022). QuasAr Odyssey: The origin of fluorescence and its voltage sensitivity in microbial rhodopsins. *Nature Communications, 13*(1), 5501.
89. Barneschi, L., Marsili, E., Pedraza-González, L., Padula, D., De Vico, L., Kaliakin, D., Blanco-González, A., Ferré, N., Huix-Rotllant, M., Filatov, M., & Olivucci, M. (2022). On the fluorescence enhancement of arch neuronal optogenetic reporters. *Nature Communications, 13*(1), 6432.